

Design, Development and Implementation of Controller for the Wheel Hub BLDC Motor in an Electric Scooter

*A Thesis Submitted in Partial Fulfilment of the Requirements
for the Degree of*

MASTER OF TECHNOLOGY

By

TABREJ ALAM

(Roll no. 224102113)

Under the Supervision of

Dr. Praveen Tripathy



Department of Electronics and Electrical Engineering
Indian Institute of Technology Guwahati
Guwahati - 781 039, India

June 2024

Certificate

This is to certify that the thesis entitled "**Design, Development and Implementation of Controller for the Wheel Hub BLDC Motor in an Electric Scooter**", submitted by **Mr Tabrej Alam (Roll no.-224102113)**, a master student in the *Department of Electronics and Electrical Engineering, Indian Institute of Technology Guwahati*, for the award of the degree of **Master of Technology**, is a record of an original research work carried out by him under my supervision and guidance. The thesis has fulfilled all requirements as per the regulations of the institute and has reached the standard needed for submission. The results embodied in this thesis have not been submitted to any other University or Institute for the award of any degree or diploma.

Dated: June, 2024
Guwahati.

Dr. Praveen Tripathy
Associate Professor
Dept. of Electronics and Electrical Engg.
Indian Institute of Technology Guwahati
Guwahati - 781 039, Assam, India.

Acknowledgement

I thank my supervisor ***Dr. Praveen Tripathy*** for giving me the opportunity to work on the project titled **Design, Development and Implementation of Controller for the Wheel Hub BLDC Motor in an Electric Scooter.**

I extend my sincere gratitude to my committee members ***Dr. Ravindranath Adda*** and ***Dr. Sreenath J.G.*** for their continuous oversight and invaluable guidance throughout the duration of the project.

I am also thankful to my department colleagues and seniors, especially ***Dr. Tako Nama***, for her continuous guidance throughout the course of the project.

Finally, I extend my heartfelt gratitude to my family members. Their unwavering support, encouragement, and understanding have been a source of strength throughout this journey.

Tabrej Alam

Abstract

The global trend towards sustainable urban mobility has highlighted the need for innovative solutions in electric transportation. The change in perspective has resulted in the growth of electric scooters, which offer an efficient and environmentally responsible alternative to traditional modes of transportation. This project focuses on the design, development, and implementation of a sophisticated controller for the Brushless Direct Current (BLDC) motor integrated into the wheel hub which is used to drive an electric scooter.

This thesis focuses on the comprehensive analysis, simulation, and control of Brushless DC (BLDC) motors, which are pivotal to the project's objectives. The report begins with a theoretical examination of BLDC motor operation in both trapezoidal and sinusoidal commutation modes. Subsequently, it delves into various controller design techniques, detailing the implementation of closed-loop control methods such as DC current control, Field Oriented Control (FOC), and hysteresis control. The final sections cover the hardware implementation of BLDC motor speed control, utilising the Waijung Blockset and the STM32 microcontroller, in both open-loop and closed-loop configurations. This holistic approach ensures a robust understanding and practical application of BLDC motor control strategies.

BLDC motors have gained popularity in a variety of industrial applications due to their high efficiency, low maintenance requirements, compact design, regenerative braking capabilities, precise control, durability, and compatibility with digital communication protocols, all of which contribute to the overall performance and sustainability of electric mobility. However, obtaining optimal speed

regulation under varied operating conditions remains a difficult task.

Overall, This project aims to design a controller by implementing different control strategies to ensure the satisfactory closed loop operation of the wheel hub BLDC motor. The outcomes of this project are expected to enhance the efficiency, performance, and user experience of electric scooters, fostering a sustainable and eco-friendly urban transportation landscape

Contents

List of Figures	xiii
List of Tables	xvii
List of Acronyms	xix
1 Introduction	1
1.1 Introduction	2
2 Literature Review	5
2.1 Introduction	6
2.2 Modeling of PM Brushless DC Motor	6
2.2.1 Model of BLDC Motor in DQ Reference Frame	10
2.2.2 Park's Transformation	10
2.2.3 DQ-Reference Frame Modeling	10
2.3 The 120° Conduction Mode	11
2.3.1 Different Modes of Operation in 120° Commutation	12
2.3.2 Switching Logic of 120° Commutation Mode	14
2.3.3 Truth Table of 120° Commutation Mode	14
2.3.4 Boolean Expression of Different Switches	15
2.3.5 Analysis For Different Modes	15
2.4 180° Conduction Mode	17
2.4.1 Different Modes of Operation in 180° Commutation	17
2.4.2 Switching Logic of 180° Conduction Mode	19
2.4.3 Truth Table of 180° Commutation Mode	20

Contents

2.4.4	Boolean Expression of Different Switches	20
2.4.5	Analysis For Different Modes	21
3	Open Loop Simulation of BLDC Motor	23
3.1	Introduction	24
3.2	H-PWM-L-ON	24
3.3	Given Parameter	25
3.4	120° Conduction Mode	25
3.4.1	Simulation Diagram	25
3.4.2	Without PWM	26
3.4.3	PWM with 0.2 Duty Ratio	26
3.4.4	PWM with 0.5 Duty Ratio	27
3.4.5	PWM with 0.7 Duty Ratio	27
3.4.6	Observation	27
3.5	180° Conduction Mode	28
3.5.1	Simulation Diagram	28
3.5.2	Without PWM	29
3.5.3	PWM with 0.5 Duty Ratio	29
3.5.4	PWM with 0.7 Duty Ratio	30
3.5.5	Observation	30
4	Controller Design and Close Loop Simulation of BLDC Motor	31
4.1	Controller Design By Ziegler-Nichols Tuning Method	32
4.1.1	First Method	32
4.1.2	Second Method	34
4.2	Close Loop Control of BLDC Motor	39
4.2.1	DC Control Technique	39
4.2.2	Controller design For Speed Loop	41
4.2.3	Controller design For Current Loop	42
4.2.4	Simulation Diagram for DC Current Control (DCC) Technique	44

4.2.5	Simulation Results	44
4.2.6	Field Oriented Control (FOC) Technique	46
4.2.7	Simulation Diagram for Field Oriented Control (FOC) technique	48
4.2.8	Simulation Results for 120° conduction	50
4.2.9	Results	50
4.2.10	Hysteresis Current Control Technique	52
4.2.11	Simulation Diagram for Hysteresis Current Control Technique	53
4.2.12	Simulation Results for 120° conduction	55
5	Hardware	57
5.1	Introduction	58
5.2	Briefs description of hardware setup	59
5.3	Hardware implemantation	61
5.3.1	Decoder Circuit	64
5.4	Open loop hardware implementation	66
5.4.1	Open loop results	68
5.5	Close loop hardware implementation	70
5.5.1	Frequency counter	72
5.5.2	Waijung Simulation	73
5.5.3	Speed range	74
5.5.4	Digital to Analog Converter (LTC2645)	75
5.5.5	Hardware Results	78
6	Conclusion and Future Scope	81
6.1	Conclusion	82
6.2	Future Work	82
Bibliography		85

Contents

List of Figures

1.1	General block diagram of operation of BLDC motor	3
2.1	Schematic of three-phase stator winding of BLDC motor	7
2.2	Mode1 operation is describe by (a) and Mode2 operation is describe by (b) .	12
2.3	Mode3 operation is describe by (a) and Mode4 operation is describe by (b) .	13
2.4	Mode5 operation is describe by (a) and Mode6 operation is describe by (b) .	13
2.5	Hall signals, switching signals, stator back EMF and stator current waveforms	16
2.6	Mode1 operation is describe by (a) and Mode2 operation is describe by (b) .	18
2.7	Mode3 operation is describe by (a) and Mode4 operation is describe by (b) .	18
2.8	Mode5 operation is describe by (a) and Mode6 operation is describe by (b) .	19
2.9	Hall signals, switching signals, stator back EMF and stator current waveforms	22
3.1	Open loop simulation diagram of 120° commutation	25
3.2	Waveform of rotor speed, stator current and back emf when there is no PWM technique is applied: (a) rotor speed (b) stator current (c) back emf	26
3.3	Waveform of rotor speed, stator current and back emf when there is PWM technique with duty ratio of 0.2 is applied: (a) rotor Speed (b) stator current (c) back emf	26
3.4	Waveform of rotor speed, stator current and back emf when there is PWM technique with duty ratio of 0.5 is applied: (a) rotor Speed (b) stator current (c) back emf	27
3.5	When PWM with 0.7 duty is applied: (a) rotor speed (b) stator current (c) back emf	27

List of Figures

3.6	Open loop simulation diagram of 180° commutation	28
3.7	Waveform of rotor speed, stator current and back emf when there is No PWM technique is applied: (a) rotor speed (b) stator current (c) back emf	29
3.8	Waveform of rotor speed, stator current and back emf when there is PWM technique with duty ratio of 0.5 is applied: (a) rotor Speed (b) stator current (c) back emf	29
3.9	When PWM with 0.7 duty is applied: (a) rotor speed (b) stator current (c) back emf	30
4.1	A step response curve for the Ziegler-Nichols Method	33
4.2	A step response curve for the Ziegler-Nichols Method	33
4.3	A step response curve for the Ziegler-Nichols Method	35
4.4	Open loop step response of the given system	36
4.5	Close loop step response for the given system	38
4.6	Block diagram of DC control technique	40
4.7	Block diagram of DC control technique	44
4.8	Waveform at 400 rpm: (a) rotor speed (b) stator current (c) back emf (d) modulating signal (e) switching pulses	45
4.9	Block diagram of proposed field oriented control scheme	47
4.10	Close loop simulation diagram for 180° commutation	49
4.11	Waveform at 400 rpm: (a) rotor speed (b) stator current (c) back emf (d) modulating signal (e) switching pulses	50
4.12	Block diagram of hysteresis current control technique	53
4.13	Close loop simulation diagram for 180° commutation	54
4.14	Waveform of rotor speed, stator current, back emf, modulating signal and back switching pulses for desired speed of 400 rpm: (a) rotor rpeed (b) stator current (c) back emf (d) modulating signal (e) switching pulses	55

5.1 (a) Motherboard which include STM32F4 discovery board (b) STM32F407G-DISCOVERY board	59
5.2 Hardware Set up	60
5.3 Overall Block Diagram Representation	63
5.4 Block Diagram of Decoder Circuit	65
5.5 Waijung simulation model for open-loop hardware implementation	67
5.6 Input side DC current for different value of duty: (a) when duty is 25% (b) when duty is 30% (c) when duty is 35% (d) when duty is 40%	68
5.7 Plot representing variation of speed with respect to duty variation	69
5.8 Waijung simulation model for close-loop hardware implementation	71
5.9 Frequency counter	73
5.10 Circuit which switches operation from open to close loop	74
5.11 Speed range in close-loop operation	75
5.12 Digital to Analog converter LTC2645	76
5.13 Pin diagram of DAC converter LTC2645	77
5.14 Battery current	78
5.15 Stator current when: (a) Speed is 160 rpm (b) Speed is 200 rpm	78
5.16 (a) Variation of speed from open loop to close loop operation (115rpm to 200rpm)(b) Speed changes in close loop (200rpm to 160rpm)	79
5.17 Speed variation from close loop to open loop and then again to close loop	79

List of Figures

List of Tables

2.1	Switching logic of 120° commutation	14
2.2	Truth table for 120° conduction	14
2.3	Switching logic of 180° commutation	19
2.4	Truth table for 180° conduction	20
3.1	Specification of BLDC motor which used in simulation	25
4.1	Ziegler–Nichols Tuning Rule Based on Step Response of Plant (First Method)	34
4.2	Ziegler–Nichols Tuning Rule Based on Critical Gain K_{cr} and Critical Period (Second Method)	35
4.3	R-H table	36

List of Tables

List of Common Abbreviations

BLDC	Brushless direct current motor
DC	Direct Current
H-PWM-L-ON	High PWM Low ON
AC	Alternating current
ADC	Analog to Digital Converter
EMF	Back electromotive force
EV	Electric Vehicle
ECU	Electric control unit
EMI	Electromagnetic interference
PMSM	Permanent magnet synchronous machines
PMBLDC	Permanent magnet brushless DC motor
PWM	Pulse Width Modulation
MATLAB	Matrix Laboratory
MOSFET	Metal Oxide Semiconductor Field Effect Transistor
RBS	Regenerative Braking Circuit
rpm	Revolution Per Minute

List of Abbreviations

1

Introduction

Contents

1.1	Introduction	2
-----	--------------	---

1. Introduction

1.1 Introduction

The continuous evolution of urban transportation towards sustainability has resulted in the rapid development of electric scooters as a feasible and environmentally beneficial means of transportation. Still, improving the performance of electric scooters is a continuous task, with particular complexities associated with the use of wheel hub Brushless Direct Current (BLDC) motors. These issues are intended to be addressed by the present thesis.

As a vital part of the electric scooter's drivetrain, the wheel hub BLDC motor necessitates special attention to achieve maximum control and efficiency. This project acknowledges that precise speed control and smooth integration depend on an intelligent and responsive controller. The goal of the research is to maximise the performance of the wheel hub BLDC motor by utilising various control strategies, such as DC current control, field-oriented control(FOC), and hysteresis control.

This project follows a methodical approach that includes theoretical study, modelling, simulation, and practical implementation. Since the BLDC motor is a key component of this project, its analysis has been conducted thoroughly. The simulation of the BLDC motor has been carried out in both open-loop and closed-loop configurations for both 120° and 180° commutation. Controller design for closed-loop operation was performed using the Ziegler-Nichols method. After obtaining satisfactory results in the simulation phase, hardware implementation was conducted using the Waijung Blockset in both open-loop and closed-loop configurations. In the hardware implementation, close loop speed control of the BLDC motor was achieved for various speed ranges.

In open loop simulation, the pulse width modulation(PWM) technique with a fixed duty ratio is incorporated in order to have better control. By varying the duty ratio from 0 to 1, changes in rotor speed, stator current, and stator back emf have been observed. Simulation has been performed in both 120° and 180° commutation mode, and power transfer capability to the load in both the conduction modes has been compared.

Theoretical analysis of close loop control techniques like DC current control, Field ori-

ented control and Hysteresis control has been done in detail. Simulation is also done in both 120° and 180° commutation modes by using field oriented control technique where the desired speed is achieved by designing the controller, which parameter is calculated by using the Ziegler Nichols method.

The final aim of this project was to get familiar with the Wajung Blockset, a Simulink blockset that can easily and automatically generate C code from MATLAB/Simulink simulation models for various microcontrollers. The Wajung Blockset uses an STM32 microcontroller as its daughter board, bypassing the coding typically done by Keil software. Using this blockset, hardware implementation was performed, achieving various speed ranges in closed-loop operation.

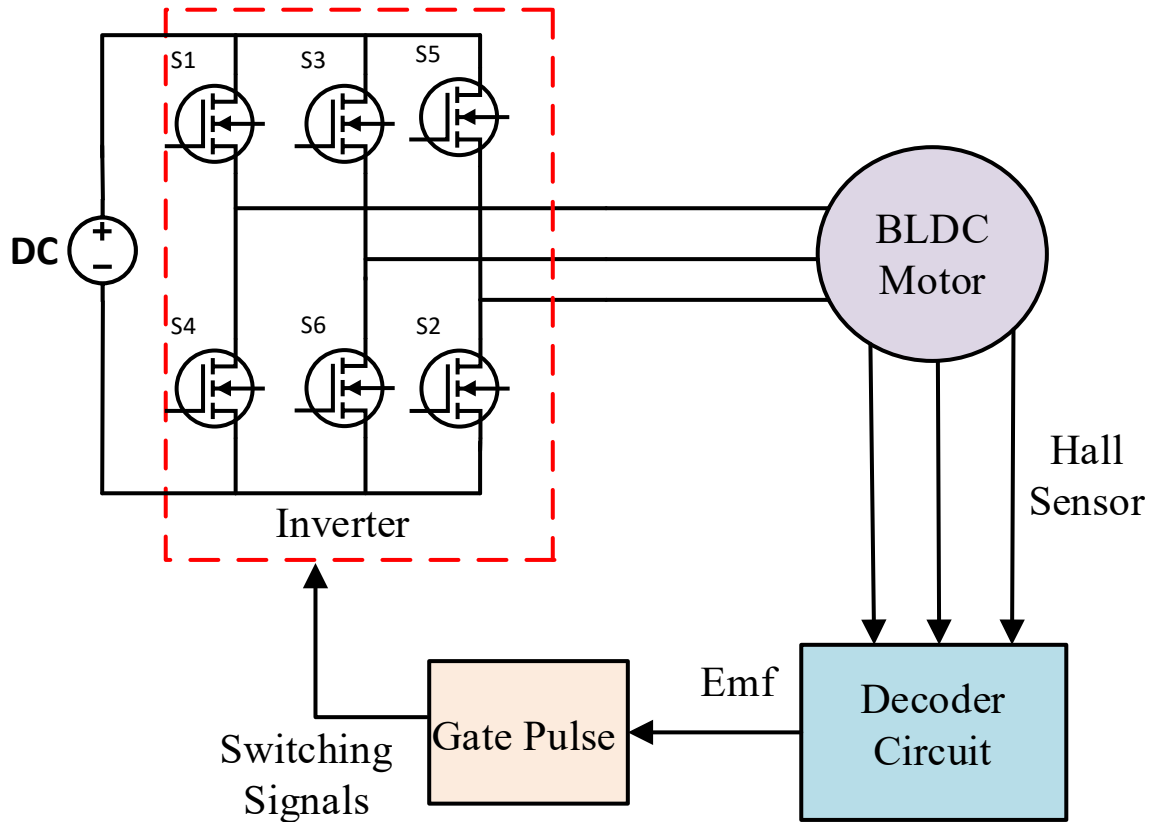


Figure 1.1: General block diagram of operation of BLDC motor

1. Introduction

2

Literature Review

Contents

2.1	Introduction	6
2.2	Modeling of PM Brushless DC Motor	6
2.3	The 120° Conduction Mode	11
2.4	180° Conduction Mode	17

2. Literature Review

2.1 Introduction

BLDC motor is the most important component in the electric scooter's powertrain. So in this section we will study about BLDC motor in detail.

The BLDC motor is a three-phase synchronous motor made up of permanent magnets in the rotor and three-phase focused windings in the stator. Due to the absence of mechanical brushes and commutator assembly, BLDC motors have less EMI difficulties and are less prone to brush wear and sparking problems than conventional dc machines [1].

Permanent Magnet Brushless DC Machines are the permanent magnet synchronous machines that have an electromotive force caused by a trapezoidal motion. The benefit of this type of permanent magnet brushless DC machine over PMSMs is its control simplicity because in this type of motor there are hall sensors which can provide the exact location of the rotor at a particular instant of time, So with information of rotor position it became easy to control the speed [2].

Due to their high efficiency, low maintenance requirements, compact design, regenerative braking capabilities, precise control, durability, and compatibility with digital communication protocols, BLDC motors have gained popularity in a variety of industrial applications, all of which contribute to the overall performance and sustainability of electric mobility. [3] obtaining optimal speed regulation under varying operating conditions, on the other hand, remains a difficult task.

2.2 Modeling of PM Brushless DC Motor

The distribution of flux in a PMBLDC motor is trapezoidal. In the context of the trapezoidal flux distribution, a phase variable model of the PMBLDC Motor makes sense. Three phase star linked stator circuit is assumed for the motor. Given that the rotor is smooth and has an angular shape, the self and mutual inductance of the three phases are equal when there is a smooth cylindrical rotor.

This model is based on the assumptions that stray and iron losses, as well as induced

currents in the rotor brought on by stator harmonic fields, are neglected. Usually, There are no damper windings in the PMBDCM. Instead, the inverter control provides damping. The motor is believed to have three stages, even though the derivation procedure can be applied to any number of phases [4].

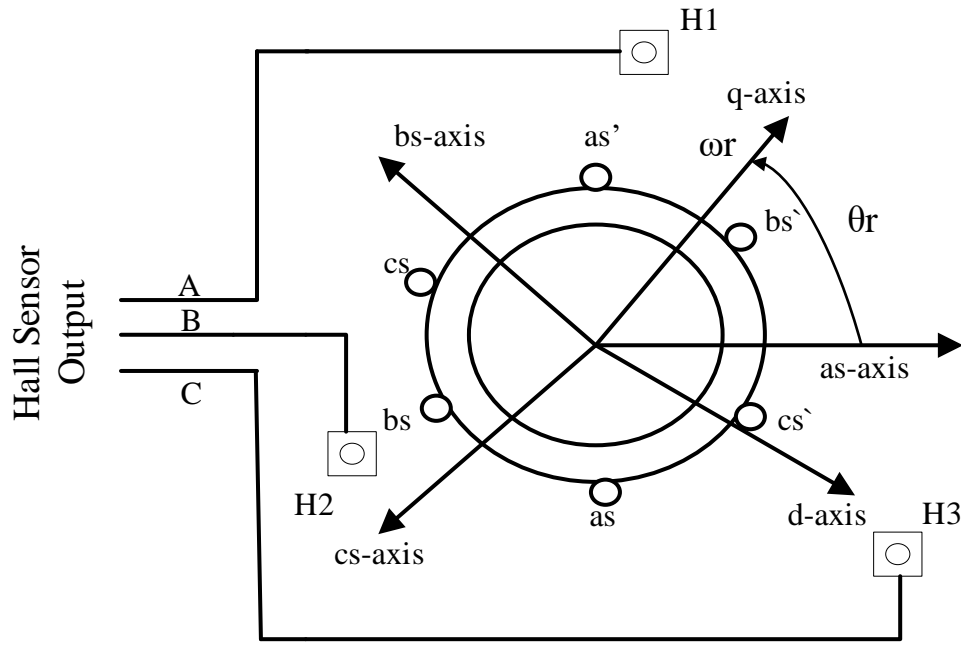


Figure 2.1: Schematic of three-phase stator winding of BLDC motor

In terms of motor electrical constants, the stator winding coupled circuit equations are given as:

$$v_{as} = R_a i_{as} + \frac{d}{dt}(L_{aa} i_{as} + L_{ba} i_{bs} + L_{ca} i_{cs}) + e_{as} \quad (2.1)$$

$$v_{bs} = R_b i_{bs} + \frac{d}{dt}(L_{ab} i_{as} + L_{bb} i_{bs} + L_{cb} i_{cs}) + e_{bs} \quad (2.2)$$

$$v_{cs} = R_c i_{cs} + \frac{d}{dt}(L_{ac} i_{as} + L_{bc} i_{bs} + L_{ca} i_{cs}) + e_{cs} \quad (2.3)$$

Writing in the matrix form of the derived coupled equations in 1.1, 1.2 and 1.3 we get,

2. Literature Review

$$\begin{bmatrix} v_{as} \\ v_{bs} \\ v_{cs} \end{bmatrix} = \begin{bmatrix} R_s & 0 & 0 \\ 0 & R_s & 0 \\ 0 & 0 & R_s \end{bmatrix} \begin{bmatrix} i_{as} \\ i_{bs} \\ i_{cs} \end{bmatrix} + p \begin{bmatrix} L_{aa} & L_{ab} & L_{ac} \\ L_{ba} & L_{bb} & L_{bc} \\ L_{ca} & L_{cb} & L_{cc} \end{bmatrix} \begin{bmatrix} i_{as} \\ i_{bs} \\ i_{cs} \end{bmatrix} + \begin{bmatrix} e_{as} \\ e_{bs} \\ e_{cs} \end{bmatrix} \quad (2.4)$$

where,

Phase voltage of stator = v_{as}, v_{bs}, v_{cs}

Stator resistance per phase = $R_a = R_b = R_c = R_s$

Self Inductance per phase = $L_{aa} = L_{bb} = L_{cc} = L_s$

Mutual Inductances = $L_{ab} = L_{bc} = L_{ca} = L_{bc} = L_{ac} = L_{cb} = M$

Stator currents = i_{as}, i_{bs}, i_{cs}

Phase back emf = e_{as}, e_{bs}, e_{cs}

Substituting the value of all variables in Equation 9.1, the PMBDCM model is obtained as:

$$\begin{bmatrix} v_{as} \\ v_{bs} \\ v_{cs} \end{bmatrix} = \begin{bmatrix} R_s & 0 & 0 \\ 0 & R_s & 0 \\ 0 & 0 & R_s \end{bmatrix} \begin{bmatrix} i_{as} \\ i_{bs} \\ i_{cs} \end{bmatrix} + p \begin{bmatrix} L & M & M \\ M & L & M \\ M & M & L \end{bmatrix} \begin{bmatrix} i_{as} \\ i_{bs} \\ i_{cs} \end{bmatrix} + \begin{bmatrix} e_{as} \\ e_{bs} \\ e_{cs} \end{bmatrix} \quad (2.5)$$

Since we know that, the stator phase currents are balanced, i.e., $i_{as} + i_{bs} + i_{cs} = 0$, So the simplification of inductance matrix in the model are given as:

$$\begin{bmatrix} v_{as} \\ v_{bs} \\ v_{cs} \end{bmatrix} = \begin{bmatrix} R_s & 0 & 0 \\ 0 & R_s & 0 \\ 0 & 0 & R_s \end{bmatrix} \begin{bmatrix} i_{as} \\ i_{bs} \\ i_{cs} \end{bmatrix} + p \begin{bmatrix} L - M & 0 & 0 \\ 0 & L - M & 0 \\ 0 & 0 & L - M \end{bmatrix} \begin{bmatrix} i_{as} \\ i_{bs} \\ i_{cs} \end{bmatrix} + \begin{bmatrix} e_{as} \\ e_{bs} \\ e_{cs} \end{bmatrix} \quad (2.6)$$

The phase voltage equation is found to be the same as the armature voltage equation of a DC machine. In industrial circles, the machine is referred to as a PM brushless dc machine because of its resemblance to a dc machine and the absence of brushes and a commutator [5].

2.2 Modeling of PM Brushless DC Motor

The electromagnetic torque is given by:

$$T_e = [e_{as}i_{as} + e_{bs}i_{bs} + e_{cs}i_{cs}] \frac{1}{w_m} \quad (N.m) \quad (2.7)$$

The instantaneous-induced emfs can be written as:

$$\begin{bmatrix} e_{as} \\ e_{bs} \\ e_{cs} \end{bmatrix} = \frac{d}{dt} \begin{bmatrix} \psi_{ra} \\ \psi_{rb} \\ \psi_{rc} \end{bmatrix} = \omega_r \lambda_p \begin{bmatrix} f_{as}(\theta_r) \\ f_{bs}(\theta_r) \\ f_{cs}(\theta_r) \end{bmatrix} \quad (2.8)$$

where,

ψ_{ra} , ψ_{rb} and ψ_{rc} is the linkage magnetic fluxes of rotor magnets with stator coils.

ω_r is the electrical angular velocity of the rotor.

λ_p is the back-EMF coefficient equal to the peak value of magnetic flux linkage.

θ_r is the electrical angular position of the rotor.

The functions $f_{as}(\theta_r)$, $f_{bs}(\theta_r)$ and $f_{cs}(\theta_r)$ have the same shape as e_{as} , e_{bs} , and e_{cs} with a maximum magnitude of ± 1 .

The induced emfs have rounded edges rather than sharp corners like those found in trapezoidal functions. The reason for this is that flux linkages are continuous functions, and since fringing also smooths out sharp edges in the flux density functions, the emfs are the derivatives of those functions. The electromagnetic torque is expressed as follows:

$$T_e = \lambda_p[f_{as}(\theta_r)i_{as} + f_{bs}(\theta_r)i_{bs} + f_{cs}(\theta_r)i_{cs}] \quad (N.m) \quad (2.9)$$

The equation of motion for a simple system with inertia J , friction coefficient B , and load torque T_l is as follows:

$$J \frac{dw_m}{dt} + B\omega_m = (T_e - T_l) \quad (2.10)$$

and electrical rotor speed and the position are related by:

$$\frac{d\theta_r}{dt} = \frac{P}{2}\omega_m \quad (2.11)$$

2. Literature Review

where,

P = number of poles

ω_m = rotor speed in mechanical rad/s

θ_r = rotor position in rad

2.2.1 Model of BLDC Motor in DQ Reference Frame

In order to transform from abc-reference frame to dq-reference frame we should have knowledge of Park's transformation.

2.2.2 Park's Transformation

The Park's transformation, which convert the ABC reference frame to the two-axis rotating dq reference frame , is used to remove time-varying stator and rotor quantities and It is defined as follows:

$$P(\theta_r) = \frac{2}{3} \begin{bmatrix} \cos(\theta_r) & \cos(\theta_r - \frac{2\pi}{3}) & \cos(\theta_r + \frac{2\pi}{3}) \\ -\sin(\theta_r) & -\sin(\theta_r - \frac{2\pi}{3}) & -\sin(\theta_r + \frac{2\pi}{3}) \end{bmatrix} \quad (2.12)$$

An inverse Park's transformation which convert the dq reference frame to the abc reference frame is given by:

$$P^{-1}(\theta_r) = \frac{2}{3} \begin{bmatrix} \cos(\theta_r) & -\sin(\theta_r) \\ \cos(\theta_r - \frac{2\pi}{3}) & -\sin(\theta_r - \frac{2\pi}{3}) \\ \cos(\theta_r + \frac{2\pi}{3}) & -\sin(\theta_r + \frac{2\pi}{3}) \end{bmatrix} \quad (2.13)$$

Zero components are neglected in the model specification because the examined motor is supposed to be a symmetrical three-phase machine [3].

2.2.3 DQ-Reference Frame Modeling

Applying the discussed Park's transformation (shown in equation 1.14) on equation (1.5), the voltage equations which are obtained for the general three-phase BLDC machine are defined as:

$$\begin{bmatrix} v_{ds}^r \\ v_{qs}^r \end{bmatrix} = \begin{bmatrix} R_s + pL_s & -\omega_r L_s \\ \omega_r L_s & R_s + pL_s \end{bmatrix} \begin{bmatrix} i_{ds}^r \\ i_{qs}^r \end{bmatrix} + P(\theta_r) \begin{bmatrix} e_{as} \\ e_{bs} \\ e_{cs} \end{bmatrix} \quad (2.14)$$

Substituting equation (1.12) and (1.8) in equation (1.14), the model of the BLOC motor is acquired, described by:

$$\begin{bmatrix} v_{ds}^r \\ v_{qs}^r \end{bmatrix} = \begin{bmatrix} R_s + pL_s & -\omega_r L_s \\ \omega_r L_s & R_s + pL_s \end{bmatrix} \begin{bmatrix} i_{ds}^r \\ i_{qs}^r \end{bmatrix} + \omega_r \lambda_p \begin{bmatrix} f_d(\theta_r) \\ f_q(\theta_r) \end{bmatrix} \quad (2.15)$$

Now the expression for electromagnetic torque in dq-reference frame can be expressed as:

$$T_e = \frac{3}{2} p [\lambda_p f_q(\theta_r) i_q + \lambda_p f_d(\theta_r) i_d] \quad (2.16)$$

The conventional model of the PMSM would be realised if function $f_q(\theta_r)$ is equal to 1 and the function $f_d(\theta_r)$ is equal to 0. And then torque expression will become:

$$T_e = \frac{3}{2} p \lambda_p i_q \quad (2.17)$$

2.3 The 120° Conduction Mode

The trapezoidal back-emf waveform of the BLDCM is typically driven by a 120° commutation and a number of control techniques. But only two windings get excited during each conduction interval, the other winding remains floating until the next conduction interval. There is always a floating winding that has no current flowing through it during each conduction interval. As a result, this floating winding does not produce any torque [6].

So the power delivered from inverter to motor in 120° conduction will be less than 120° conduction [7].

Each coil of a standard 120° commutation rotates only 120° with current to produce torque while driving a brushless DC motor; the other 60° are left idle until the next excitation. Phases A and B are conducted during the conduction period in the case of a 120°

2. Literature Review

commutation, but Phase C is not connected to either the high or low side of the inverter. Every modulation is one-sixth of an electrical period, or 60° . Every winding is conducted for 120° when it is ON [4].

2.3.1 Different Modes of Operation in 120° Commutation

- For Mode 1 and Mode 2

For mode1 switch S1 and S6 will be ON and phase C will be floating. And for mode2 switch S1 and S2 will be ON and phase B will be floating.

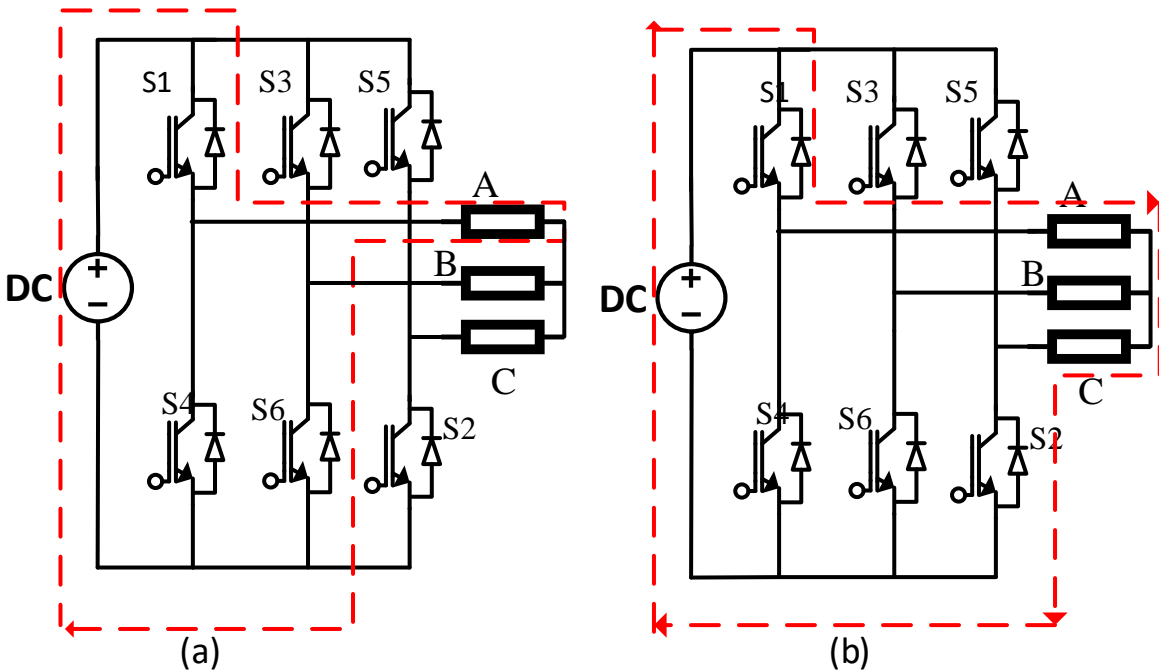


Figure 2.2: Mode1 operation is describe by (a) and Mode2 operation is describe by (b)

- For Mode3 and Mode4

For mode3 switch S5 and S2 will be ON and phase A will be floating. And for mode4 switch S3 and S4 will be ON and phase C will be floating.

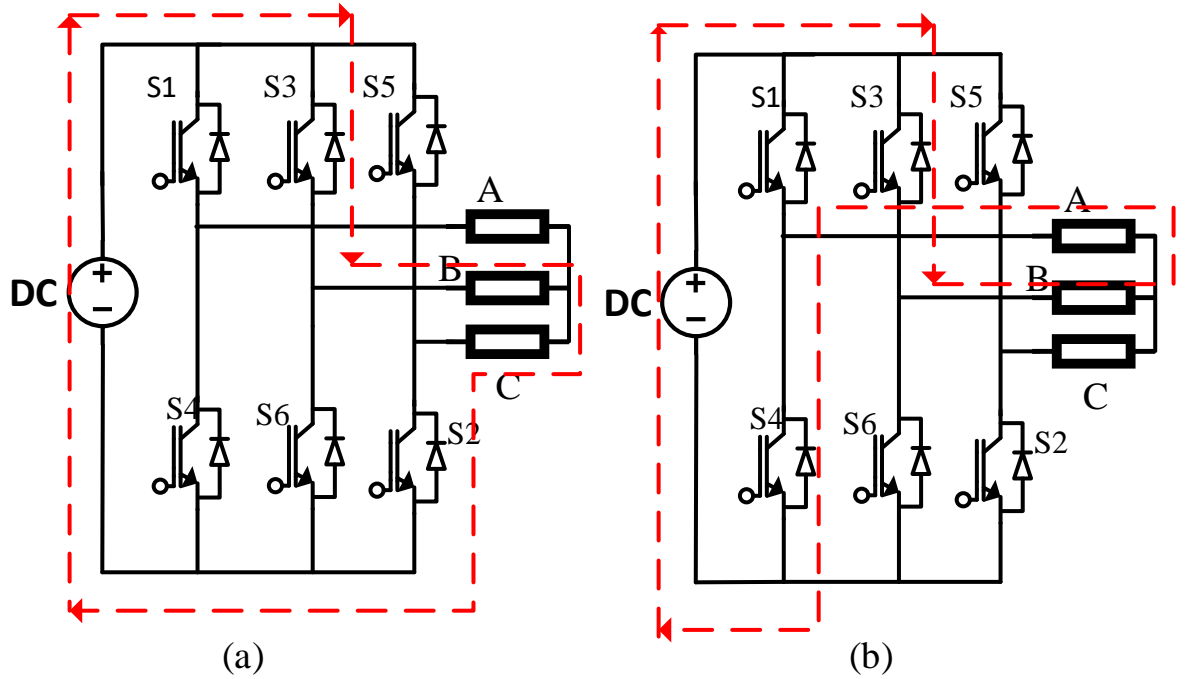


Figure 2.3: Mode3 operation is describe by (a) and Mode4 operation is describe by (b)

- **For Mode5 and Mode6**

For mode5 switch S5 and S4 will be ON and phase B will be floating. And for mode6 switch S5 and S6 will be ON and phase A will be floating.

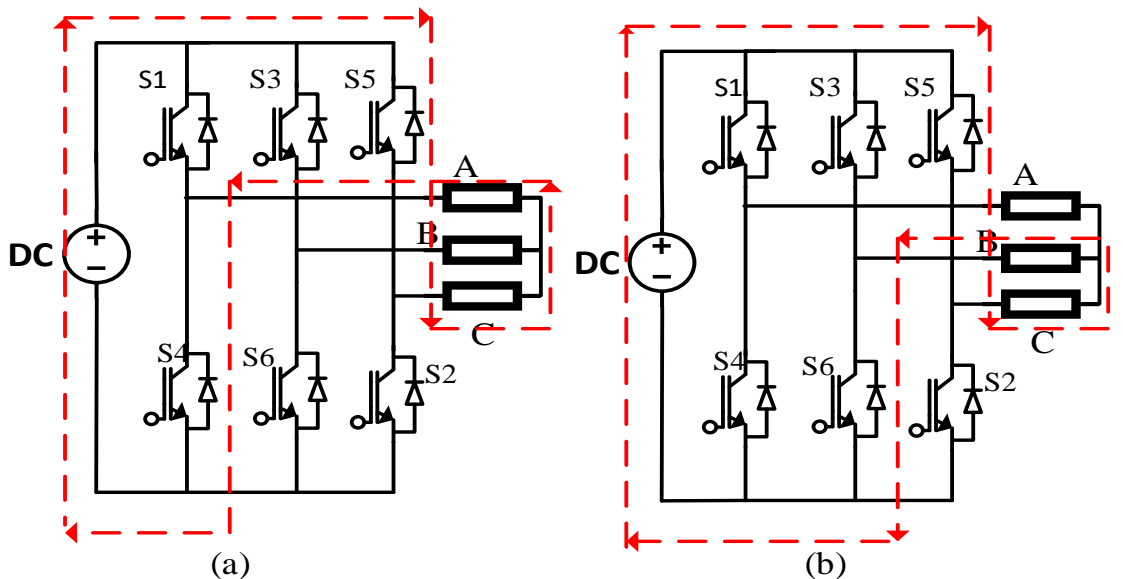


Figure 2.4: Mode5 operation is describe by (a) and Mode6 operation is describe by (b)

2. Literature Review

2.3.2 Switching Logic of 120° Commutation Mode

For 120° commutation, Each switch will be ON for 120° of interval. There will be six interval of 60° each. In each interval two switches (One from positive group switch and other from negative group switch) will be ON.

Table 2.1: Switching logic of 120° commutation

	60°	120°	180°	240°	300°	360°
S1	ON	ON				
S2		ON	ON			
S3			ON	ON		
S4				ON	ON	
S5					ON	ON
S6	ON					ON
	S1S6	S1S2	S2S3	S3S4	S4S5	S5S6

2.3.3 Truth Table of 120° Commutation Mode

Table 2.2: Truth table for 120° conduction

Mode	H_a	H_b	H_c	e_{as}	e_{bs}	e_{cs}	S1	S2	S3	S4	S5	S6
I	1	0	1	+1	-1	0	1	0	0	0	0	1
II	1	0	0	+1	0	-1	1	1	0	0	0	0
III	1	1	0	0	+1	-1	0	1	1	0	0	0
IV	0	1	0	-1	+1	0	0	0	1	1	0	0
V	0	1	1	-1	0	+1	0	0	0	1	1	0
VI	0	0	1	0	-1	+1	0	0	0	0	1	1

Where,

- H_a , H_b and H_c are the signals coming from hall effect sensors.
- e_{as} , e_{bs} and e_{cs} are the back emf induced in the motor.
- S1, S2, S3, S4, S5 and S6 are the switches of the inverter.

2.3.4 Boolean Expression of Different Switches

From the above truth table, after simplifying, we get the following simplified boolean expressions for all switches:

- $S1 = H_a \bar{H}_b$

- $S3 = H_b \bar{H}_c$

- $S5 = H_c \bar{H}_a$

- $S4 = \bar{H}_a H_b$

- $S6 = \bar{H}_b H_c$

- $S2 = \bar{H}_c H_a$

With the help of the above simplified boolean expressions, we can design a decoder circuit which can perform the 120° conduction operation.

2.3.5 Analysis For Different Modes

Each phase of the hall sensor output will be logic 1 for 180° and logic 0 for the next 180°. Hall sensor output will be same in both 120° and 180° conduction.

In 120° commutation, each switch will operate for 120 electrical degrees only and will be phase displaced by 60° each other. So in this commutation, the shape of the back emf induce will be trapezoidal in nature.

Fig. 2.5 shows the waveform of hall sensors, all switches waveform, stator back emf waveform and stator current waveform in 120°commutation.

2. Literature Review

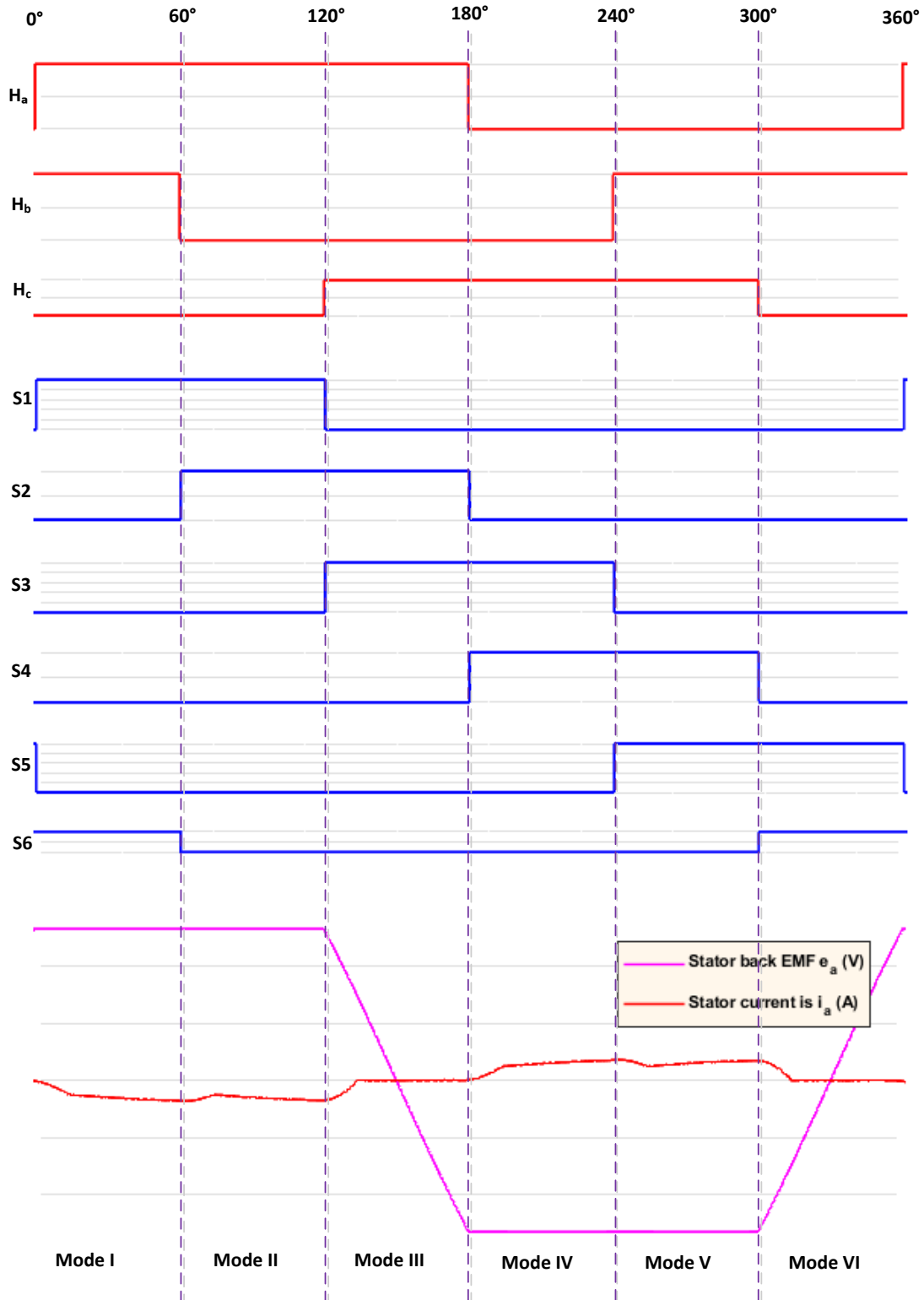


Figure 2.5: Hall signals, switching signals, stator back EMF and stator current waveforms

2.4 180° Conduction Mode

Brushless DC motors can be classified into two groups based on the conduction angle of their three-phase inverter switch: 120° and 180° conduction. 120° conduction means that each switch conducts an electrical angle of 120° during a motor cycle, while 180° conduction indicates that each switch conducts an electrical angle of 180° throughout a cycle [6]. The phase shift between any two consecutive switches will be 60 electric angles, So 180° conduction at each moment the switches will be ON.

It is possible to implement the 180° commutation as a three-phase-drive model; in that case, torque is produced in each conduction period by conducting current across all three phases. In theory, a 180° commutation system should produce a higher maximum torque than a traditional 120° commutation system [8].

So, at a particular instant, three switches are operating at a time, which means there will be no phase floating in any instant. This is the main difference in 120° and 180° conduction mode because in 120° conduction mode, at any instant, only two phases will be operating, and the third phase will be floating [9].

2.4.1 Different Modes of Operation in 180° Commutation

- **For Mode 1 and Mode 2**

For mode1 switch S1, S5 from a positive group of switches and S6 from a negative group of switches will be ON. For mode 2, S1 from a positive group of switches, and S2, S6 from a negative group of switches will be ON.

2. Literature Review

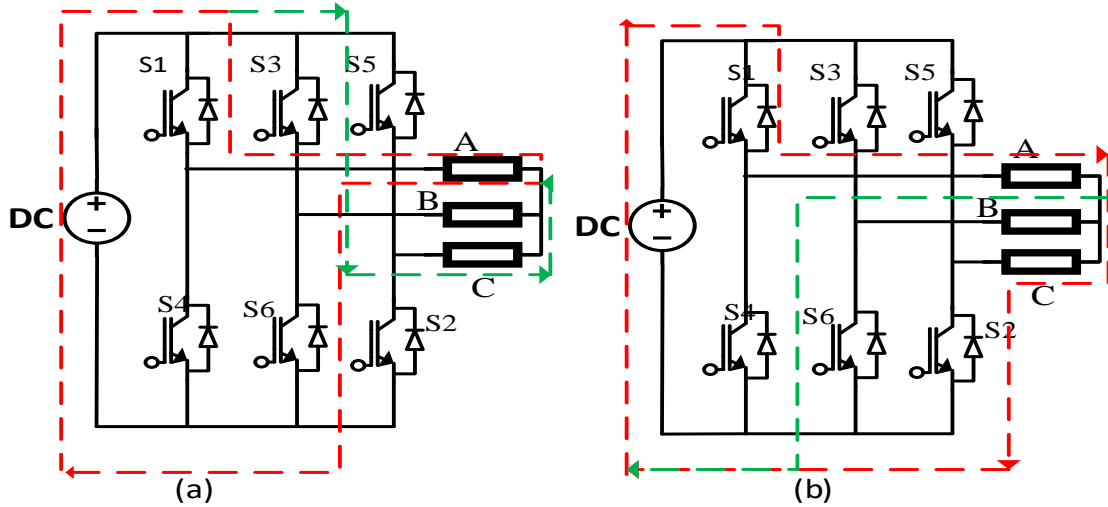


Figure 2.6: Mode1 operation is describe by (a) and Mode2 operation is describe by (b)

- **For Mode3 and Mode4**

For mode 3, switch S1 and S3 from a positive group of switches and S2 from a negative group of switches will be ON. For mode 4, S3 from a positive group of switches and S2, S4 from a negative group of switches will be ON.

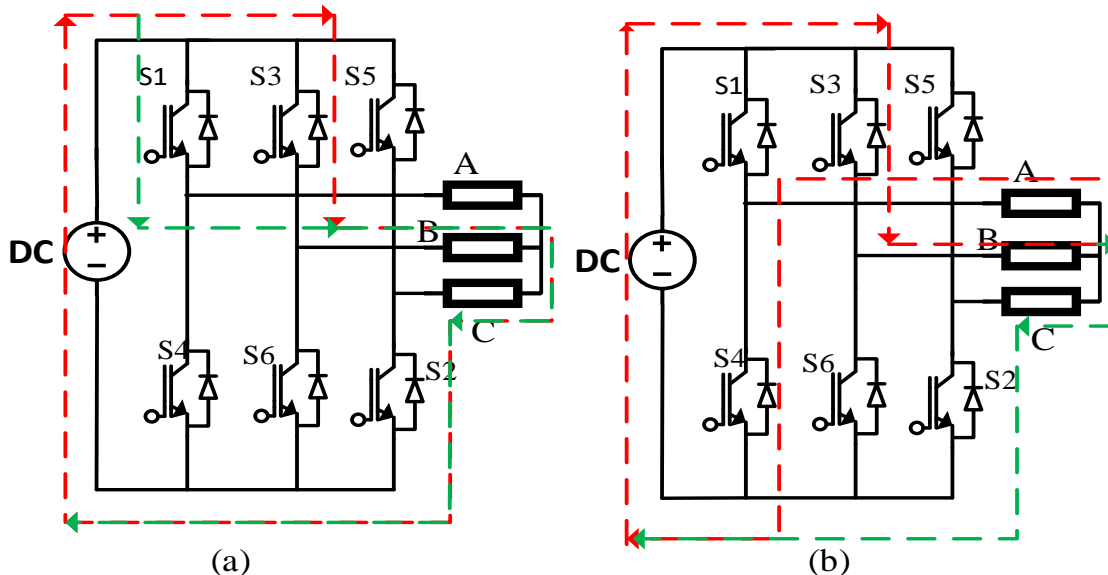


Figure 2.7: Mode3 operation is describe by (a) and Mode4 operation is describe by (b)

- **For Mode5 and Mode6**

For mode5 switch S3, S5 from a positive group of switches and S4 from a negative

group of switches will be ON. For mode 4, S5 from a positive group of switches and S4, S6 from a negative group of switches will be ON.

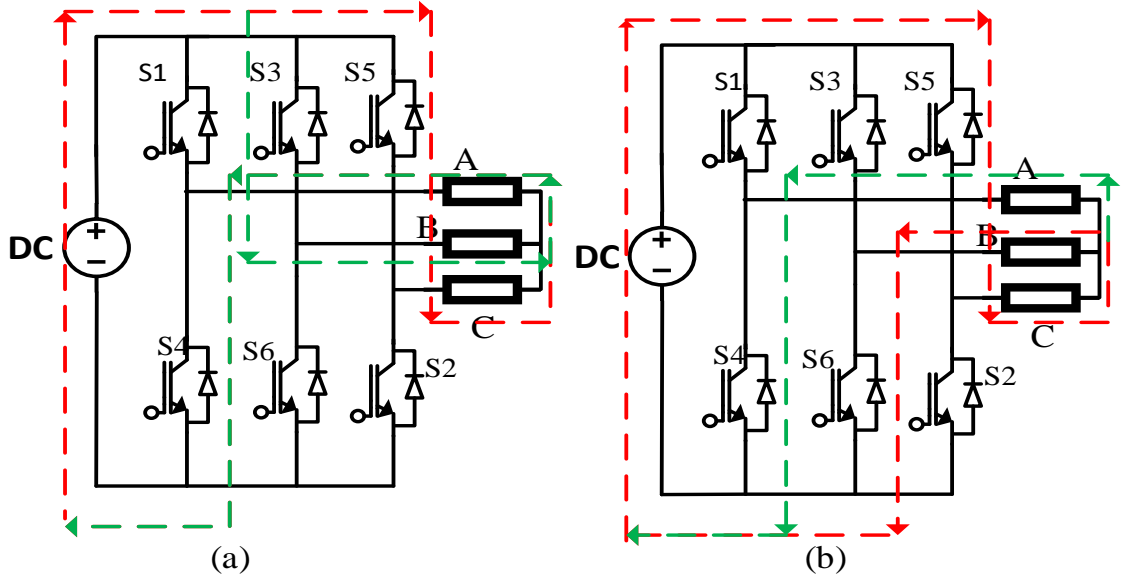


Figure 2.8: Mode5 operation is describe by (a) and Mode6 operation is describe by (b)

2.4.2 Switching Logic of 180° Conduction Mode

For 180° commutation, Each switch will be ON for 180° interval. There will be six intervals of 60° each. In each interval, three switches (either one from the positive group and two from the negative group switch or two from the positive group and one from the negative group switch) will be ON. For this type of commutation, there will be no floating switch in any mode.

Table 2.3: Switching logic of 180° commutation

	60°	120°	180°	240°	300°	360°
S1	ON	ON	ON			
S2		ON	ON	ON		
S3			ON	ON	ON	
S4				ON	ON	ON
S5	ON				ON	ON
S6	ON	ON				ON
	S1S5S6	S1S2S6	S1S2S3	S2S3S4	S3S4S5	S4S5S6

2. Literature Review

2.4.3 Truth Table of 180° Commutation Mode

Table 2.4: Truth table for 180° conduction

Mode	H_a	H_b	H_c	e_{as}	e_{bs}	e_{cs}	S1	S2	S3	S4	S5	S6
I	1	0	1	+1	-1	+1	1	0	0	0	1	1
II	1	0	0	+1	-1	-1	1	1	0	0	0	1
III	1	1	0	+1	+1	-1	1	1	1	0	0	0
IV	0	1	0	-1	+1	-1	0	1	1	1	0	0
V	0	1	1	-1	+1	+1	0	0	1	1	1	0
VI	0	0	1	-1	-1	+1	0	0	0	1	1	1

Where,

- H_a , H_b and H_c are the signals coming from hall effect sensors.
- e_{as} , e_{bs} and e_{cs} are the back emf induced in the motor.
- S1, S2, S3, S4, S5 and S6 are the switches of the inverter.

2.4.4 Boolean Expression of Different Switches

From the above truth table, after simplifying, we get the following simplified boolean expressions for all switches:

- $S1 = H_a(\bar{H}_b + \bar{H}_c)$
- $S3 = H_b(\bar{H}_a + \bar{H}_c)$
- $S5 = H_c(\bar{H}_a + \bar{H}_b)$
- $S4 = \bar{H}_a(H_b + H_c)$
- $S6 = \bar{H}_b(H_a + H_c)$
- $S2 = \bar{H}_c(H_a + H_b)$

With the help of the above simplified boolean expressions, we can design a decoder circuit which can perform the 180° conduction operation.

2.4.5 Analysis For Different Modes

Each phase of the hall sensor output will be logic 1 for 180° and logic 0 for the next 180°. Hall sensor output will be the same in both 120° and 180° conduction.

In 180° commutation, each switch will operate for 180 electrical degrees and will be phase displaced by 60° to each other. So in this commutation, the shape of the back emf induced will be sinusoidal in nature.

Fig. 1.11 show the waveform of hall sensors, all switches waveform, stator back emf waveform and stator current waveform in 180° commutation.

2. Literature Review

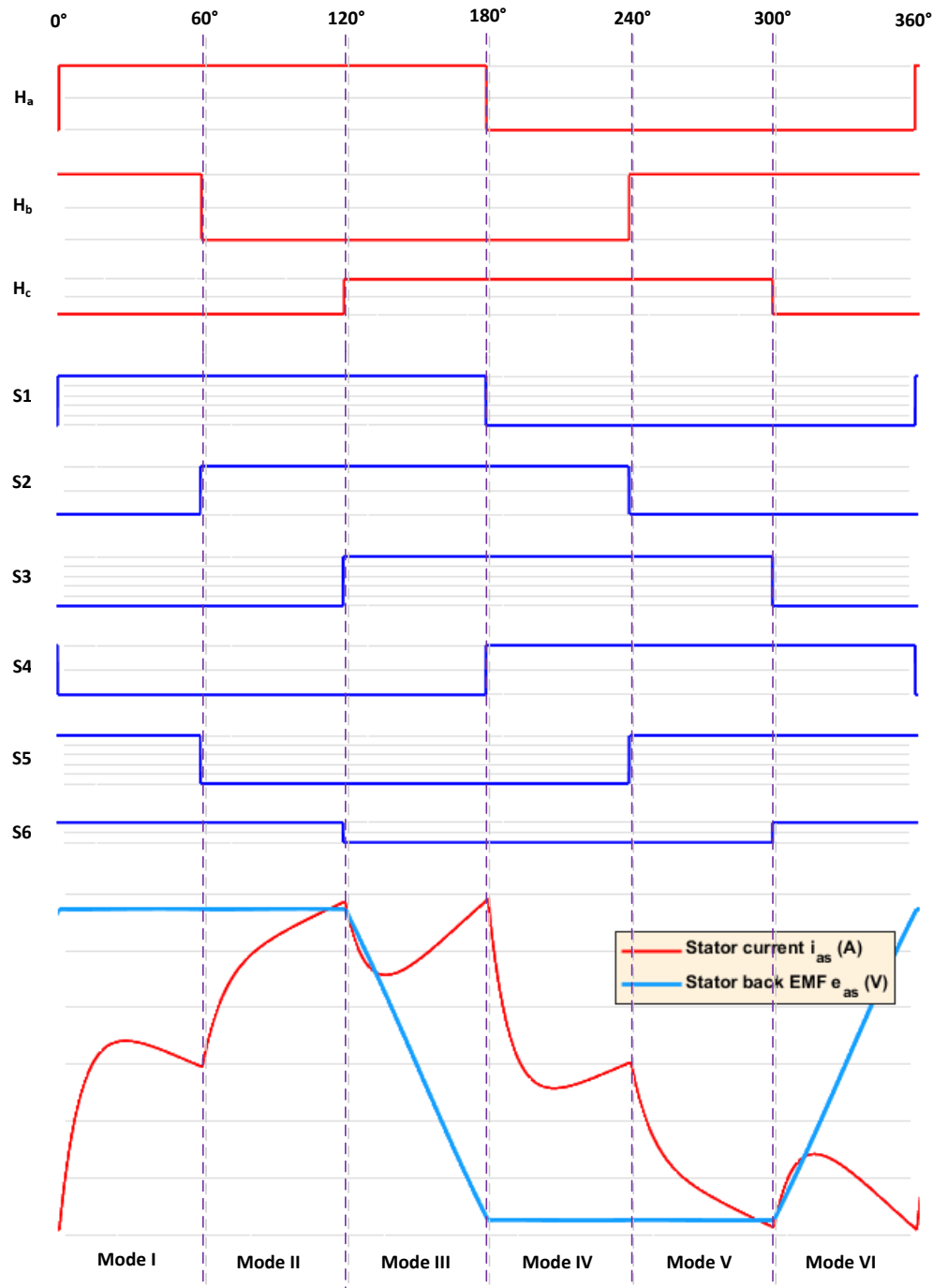


Figure 2.9: Hall signals, switching signals, stator back EMF and stator current waveforms

3

Open Loop Simulation of BLDC Motor

Contents

3.1	Introduction	24
3.2	H-PWM-L-ON	24
3.3	Given Parameter	25
3.4	120° Conduction Mode	25
3.5	180° Conduction Mode	28

3. Open Loop Simulation of BLDC Motor

3.1 Introduction

In this chapter, we will implement the open loop simulation of the BLDC motor in both 120° conduction and in 180° conduction mode. Analysing a Brushless DC (BLDC) motor's behaviour without feedback control is known as open-loop simulation. The motor receives the control input in an open-loop system, but there is no way to monitor the output or offer feedback for adjustment [10].

To get control over speed and torque, we are also implementing a pulse width modulation technique along with open loop simulation. In this, we are giving a fixed duty ratio, and for this duty ratio, we are generating a modulating signal, and then these signals are given to the switches of the inverter. we are using AND gate to combine the effect of electronic commutation as well as PWM [7].

Understanding the fundamental behaviour of the BLDC motor requires the use of open-loop simulations, which may also be used as a basis for the creation of closed-loop control schemes later in the project.

3.2 H-PWM-L-ON

In this type of pulse width modulation (PWM), the PWM technique will be applied to only positive groups of switches like S1, S3 and S5. And the negative group of switches like S2, S4, and S6 will remain ON throughout the cycle.

The six PWM methods that are usually utilised by the voltage inverter in BLDC motor speed control are H-PWM-L-PWM, ON-PWM, H-PWM-L-ON, H-ON-L-PWM, PWM-ON, and PWM-ON-PWM. [11]. But in this project, we will use the H-PWM-L-ON scheme due to the advantage of getting the smallest torque ripple due to the current commutation.

3.3 Given Parameter

Table 3.1: Specification of BLDC motor which used in simulation

Parameter	R	L	J	D	Pole	K_b
Value	0.36Ω	0.4 mH	0.008 kg/m^2	0.001	24	100

3.4 120° Conduction Mode

3.4.1 Simulation Diagram

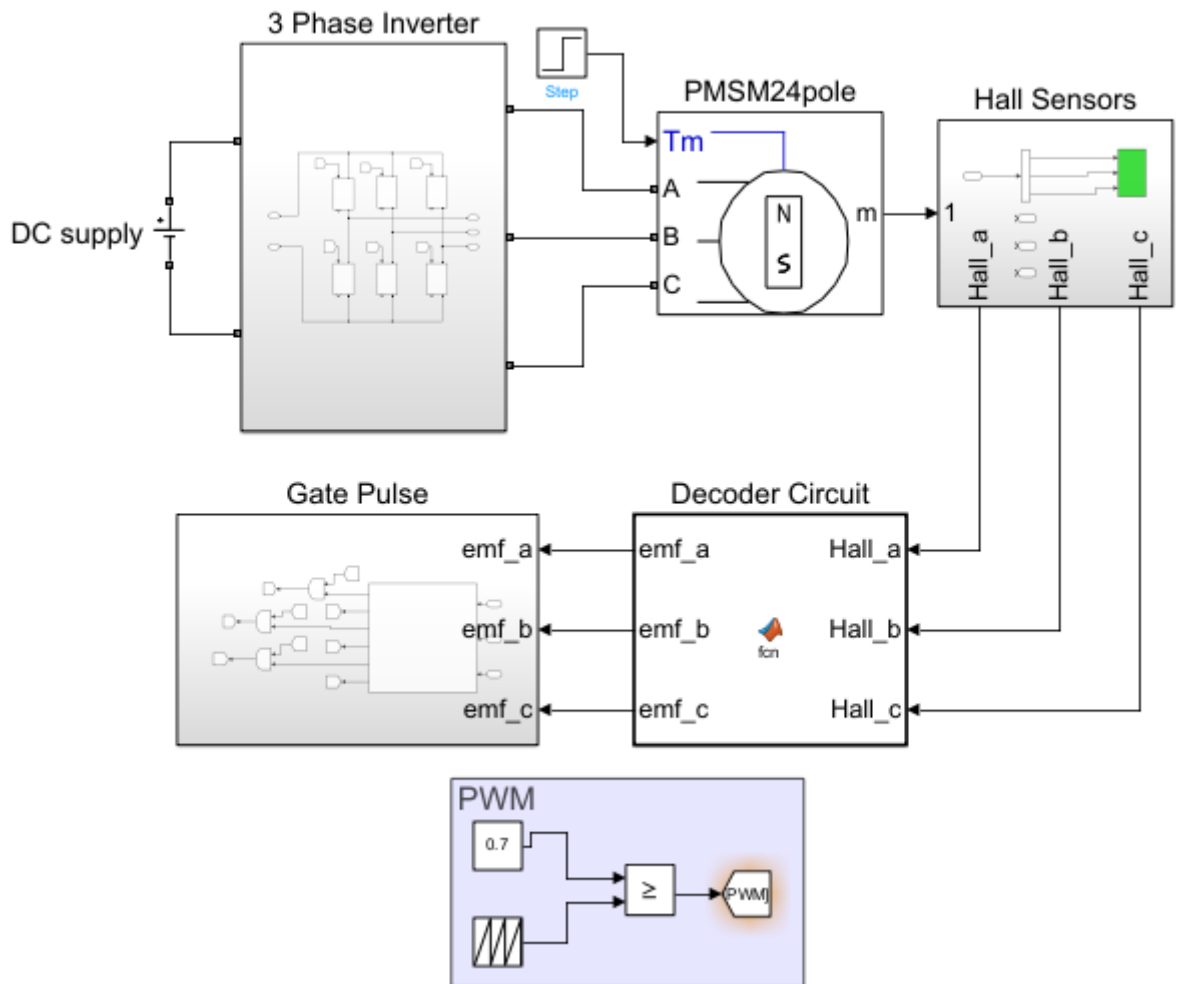


Figure 3.1: Open loop simulation diagram of 120° commutation

3. Open Loop Simulation of BLDC Motor

3.4.2 Without PWM

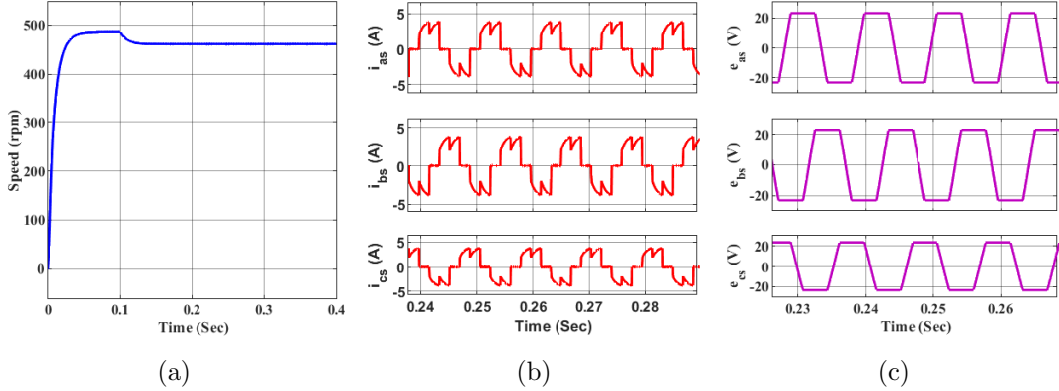


Figure 3.2: Waveform of rotor speed, stator current and back emf when there is no PWM technique is applied: (a) rotor speed (b) stator current (c) back emf

3.4.3 PWM with 0.2 Duty Ratio

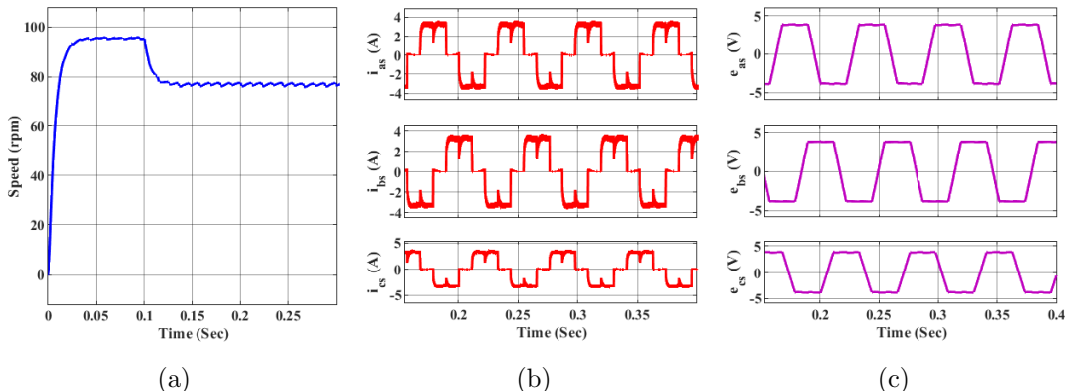


Figure 3.3: Waveform of rotor speed, stator current and back emf when there is PWM technique with duty ratio of 0.2 is applied: (a) rotor Speed (b) stator current (c) back emf

3.4.4 PWM with 0.5 Duty Ratio

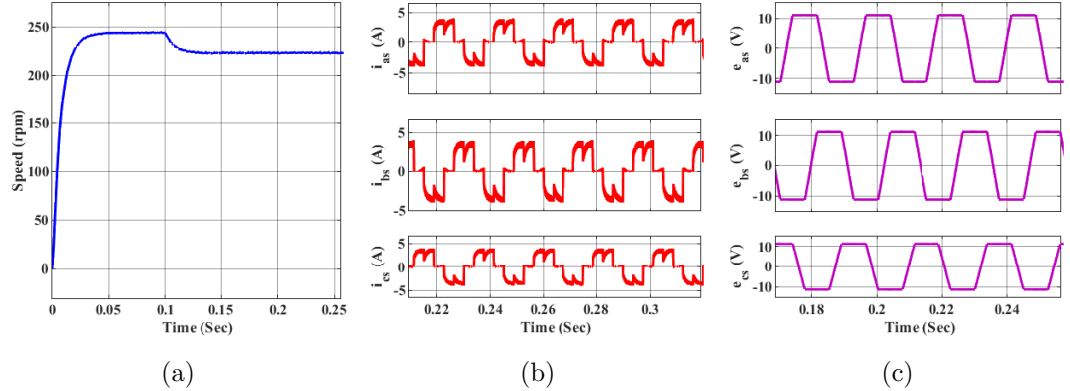


Figure 3.4: Waveform of rotor speed, stator current and back emf when there is PWM technique with duty ratio of 0.5 is applied: (a) rotor Speed (b) stator current (c) back emf

3.4.5 PWM with 0.7 Duty Ratio

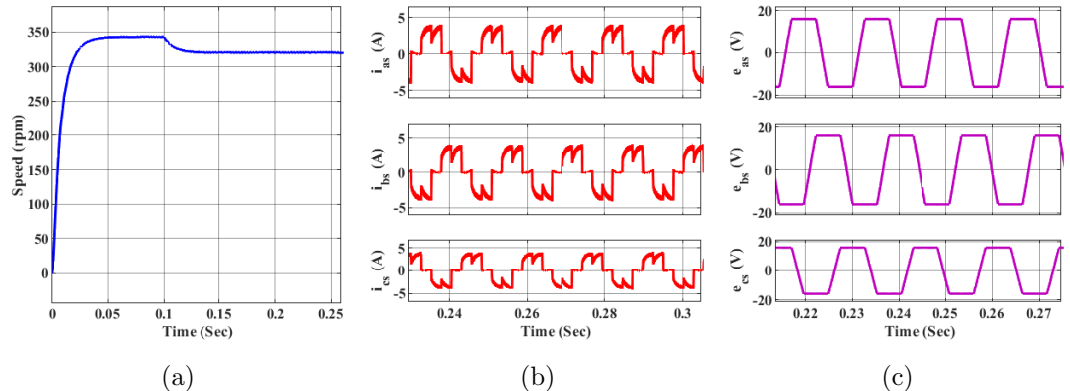


Figure 3.5: When PWM with 0.7 duty is applied: (a) rotor speed (b) stator current (c) back emf

3.4.6 Observation

- We are getting maximum speed as well as very less ripple in speed and current when operating in the No PWM mode. But there is no variation in speed.
- As the duty ratio of PWM increases, the speed of the motor increases.
- With PWM, we have more control over a range of speeds.

3. Open Loop Simulation of BLDC Motor

3.5 180° Conduction Mode

3.5.1 Simulation Diagram

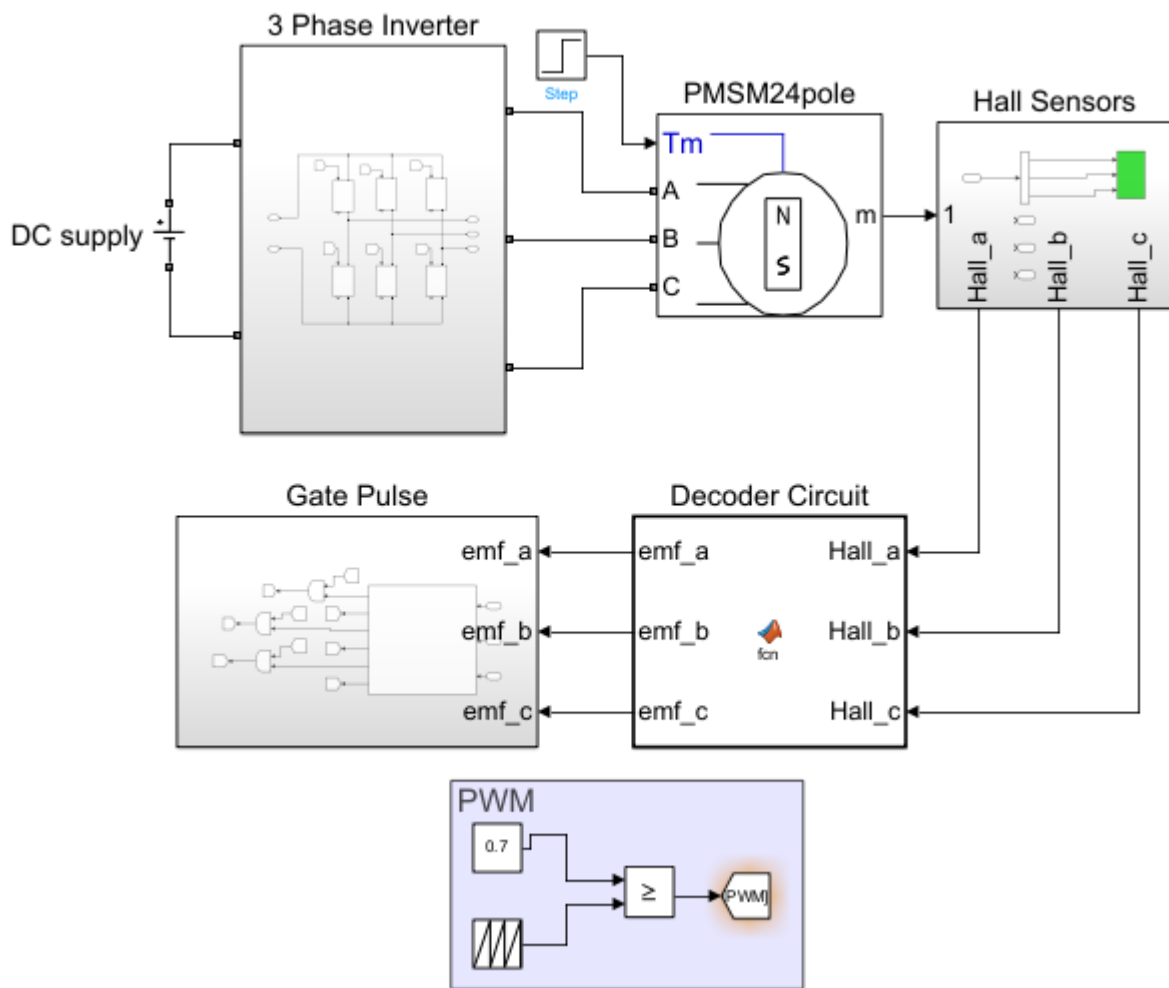


Figure 3.6: Open loop simulation diagram of 180° commutation

3.5.2 Without PWM

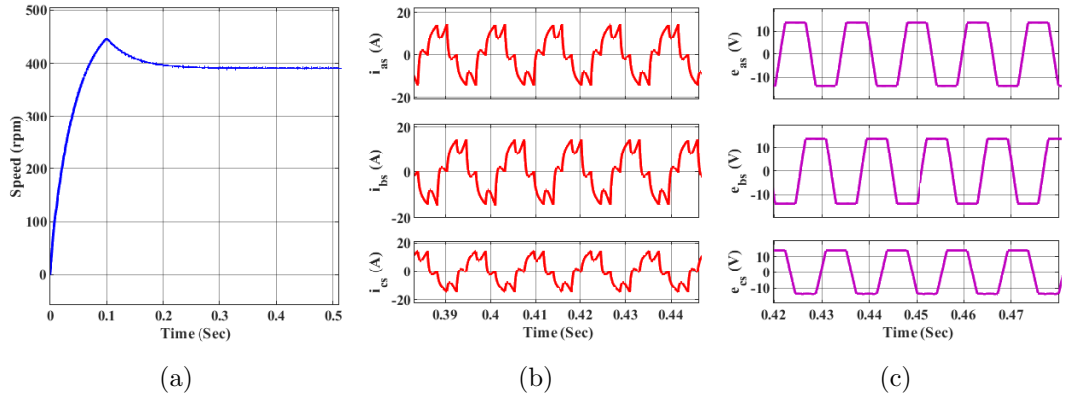


Figure 3.7: Waveform of rotor speed, stator current and back emf when there is No PWM technique is applied: (a) rotor speed (b) stator current (c) back emf

3.5.3 PWM with 0.5 Duty Ratio

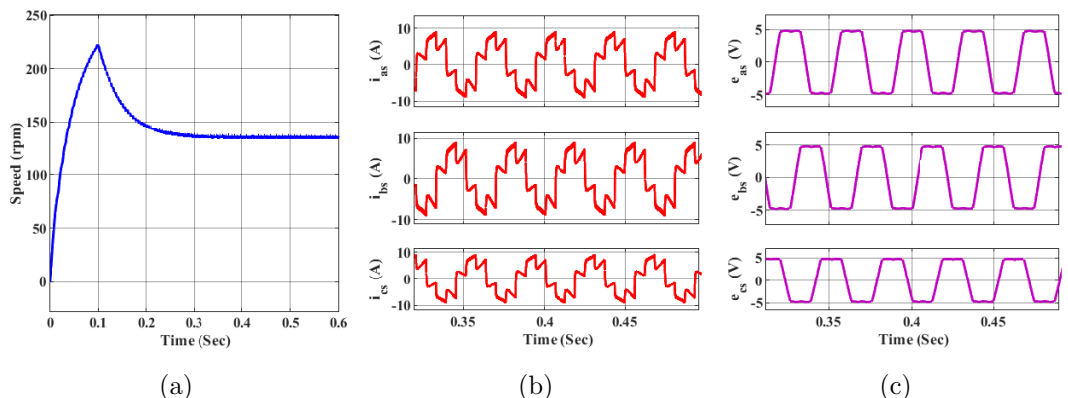


Figure 3.8: Waveform of rotor speed, stator current and back emf when there is PWM technique with duty ratio of 0.5 is applied: (a) rotor Speed (b) stator current (c) back emf

3. Open Loop Simulation of BLDC Motor

3.5.4 PWM with 0.7 Duty Ratio

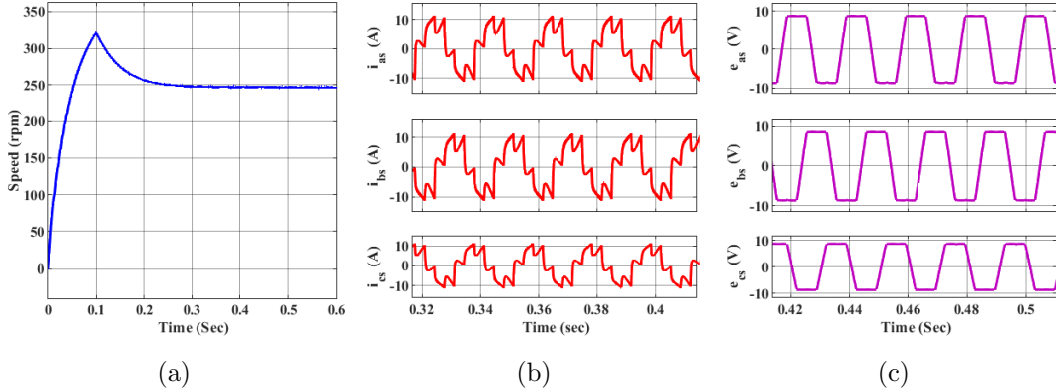


Figure 3.9: When PWM with 0.7 duty is applied: (a) rotor speed (b) stator current (c) back emf

3.5.5 Observation

- We are getting maximum speed as well as very less ripple in speed and current when operating in the No PWM mode. But there is no variation in speed.
- As the duty ratio of PWM increases, the speed of the motor increases.
- With PWM, we have more control over a range of speeds.

4

Controller Design and Close Loop Simulation of BLDC Motor

Contents

4.1	Controller Design By Ziegler-Nichols Tuning Method	32
4.2	Close Loop Control of BLDC Motor	39

4.1 Controller Design By Ziegler-Nichols Tuning Method

The process of selecting the controller parameters to meet given performance specifications is known as controller tuning. Ziegler and Nichols suggested rules for tuning PID controllers (meaning to set values) based on experimental step responses or based on the value that results in marginal stability when only proportional control action is used. These rules suggest a set of values of K_P , T_I , and T_D , and that will give a stable operation of the system. However, the resulting system may exhibit a large maximum overshoot in the step response, which is unacceptable. In such a case, we need a series of fine tunings until an acceptable result is obtained. In fact, the Ziegler–Nichols tuning rules give an educated guess for the parameter values and provide a starting point for fine-tuning, rather than giving the final settings for and in a single shot [12].

Ziegler and Nichols proposed rules for determining values of the proportional gain integral time and derivative time based on the transient response characteristics of a given plant. Such determination of the parameters of PID controllers or tuning of PID controllers can be made by engineers on-site by experiments on the plant.

There are two methods called Ziegler–Nichols tuning rules: the first method and the second method. We shall give a brief presentation of these two methods.

4.1.1 First Method

In the first method, we obtain the response of the plant to a unit-step input, as shown in Figure 4.1. If the plant involves neither integrator(s) nor dominant complex-conjugate poles, then such a unit-step response curve may look S-shaped, as shown in Figure 4.2. This method applies if the response to a step input exhibits an S-shaped curve. Such step-response curves may be generated experimentally or from a dynamic simulation of the plant.

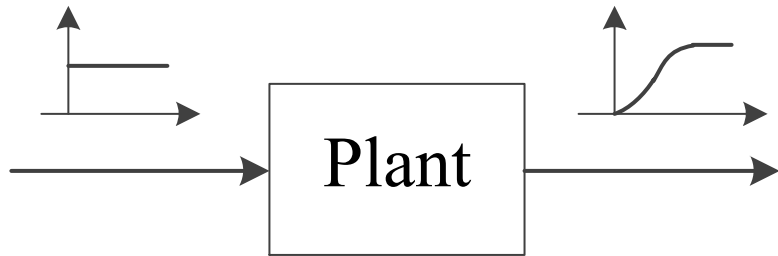


Figure 4.1: A step response curve for the Ziegler-Nichols Method

The S-shaped curve may be characterized by two constants, delay time L and time constant T . The delay time and time constant are determined by drawing a tangent line at the inflection point of the S-shaped curve and determining the intersections of the tangent line with the time axis and line $c(t)=K$, as shown in Figure 4.2.

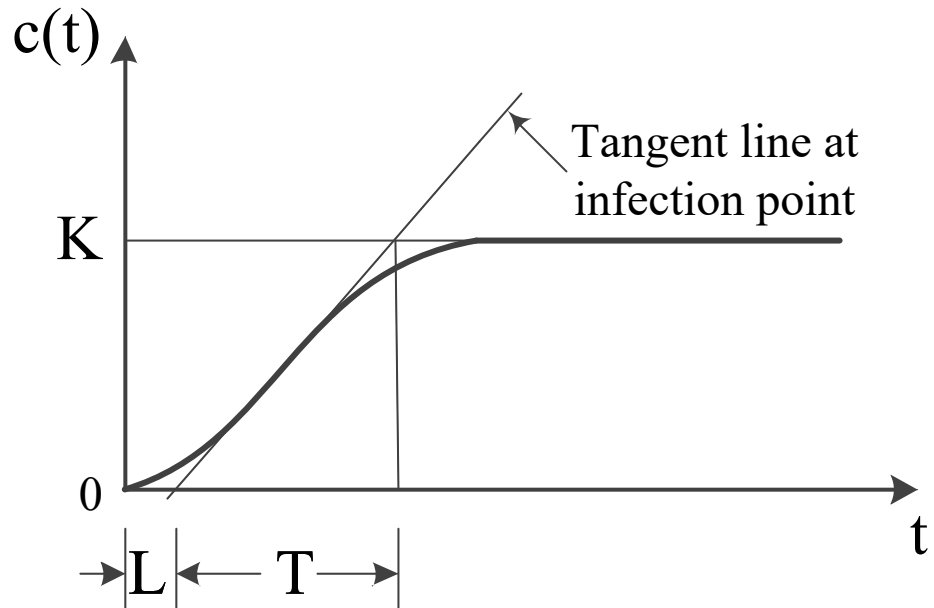


Figure 4.2: A step response curve for the Ziegler-Nichols Method

The transfer function $C(s)/U(s)$ may then be approximated by a first-order system with a transport lag as follows:

$$\frac{C(s)}{U(s)} = \frac{Ke^{-Ls}}{Ts + 1} \quad (4.1)$$

Ziegler and Nichols suggested to set the values of L and T according to the formula shown in Table 4.1 as shown below:

4. Controller Design and Close Loop Simulation of BLDC Motor

Table 4.1: Ziegler–Nichols Tuning Rule Based on Step Response of Plant (First Method)

Types of Controller	K_P	$T_I = \frac{K_P}{K_I}$	$T_D = \frac{K_D}{K_P}$
P	$\frac{T}{L}$	∞	0
PI	$0.9\frac{T}{L}$	$\frac{L}{0.3}$	0
PID	$1.2\frac{T}{L}$	2L	0.5L

Finally, with the help of the above table, the value of K_P , K_I , and K_D can be calculated.

4.1.2 Second Method

In the second method, we first set and Using the proportional control action only (see Figure 4.3), increase K_p from 0 to a critical value K_{cr} at which the output first exhibits sustained oscillations. (If the output does not exhibit sustained oscillations for whatever value K_p may take, then this method does not apply.) Thus, the critical gain K_{cr} and the corresponding period are experimentally determined (see Figure 4.3). Ziegler and Nichols suggested that we set the values of the parameters according to the formula shown in Table 4.2.

This technique suggested that Reducing the gains by a suitable factor comes after increasing the gain till the system begins to oscillate [13].

The steps for the Ziegler-Nichols Tuning Method are as follows:

- First calculate the transfer function of the plant
- Add PI or PID controller and make all gain zero except K_p
- Now, with the help of R-H stability criteria, find out the value of $K_p = K_{cr}$ for which the system will oscillate. If oscillation doesn't happen, we need to try another approach.
- Put obtained value of K_p (all other gains are still zero) and find out unit step response.
- From the unit step response find out the time period of oscillation P_{ccr}
- Then find the value of K_I and K_D using below table.

4.1 Controller Design By Ziegler-Nichols Tuning Method

where,

K_{cr} = critical gain (maximum positive gain) of K_p

P_{cr} = Time period of step response

Table 4.2: Ziegler–Nichols Tuning Rule Based on Critical Gain K_{cr} and Critical Period (Second Method)

Types of Controller	K_P	$T_I = \frac{K_P}{K_I}$	$T_D = \frac{K_D}{K_P}$
P	$0.5K_{crit}$	∞	0
PI	$0.45K_{crit}$	$\frac{1}{1.2}P_{crit}$	0
PID	$0.6K_{crit}$	$0.5P_{crit}$	$0.125P_{crit}$

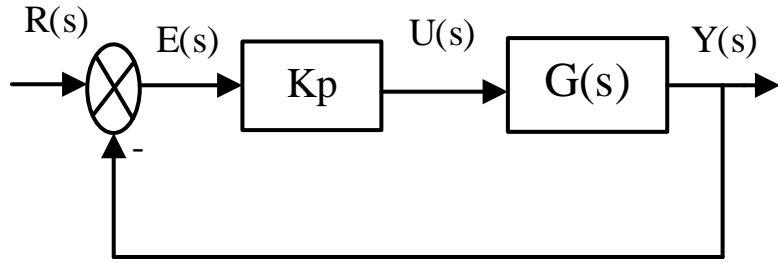


Figure 4.3: A step response curve for the Ziegler-Nichols Method

In order to find out the critical value of K_P and P_{cr} we have to use the concept of R H Criteria as follows:

- Find out characteristics equation, $1 + G(s).H(s) = 0$
- From R H table make coefficient of $s_1 = 0$ and find out K_{cr} .
- Now from auxiliary polynomial and find value of P_{cr} by using the value of K_{cr} [14].

Lets understand with the example. Suppose we have third order system with a plant transfer function,

$$G(s) = \frac{1}{(s+1)(s+3)(s+5)}$$

Open loop step response of the given transfer function is:

4. Controller Design and Close Loop Simulation of BLDC Motor

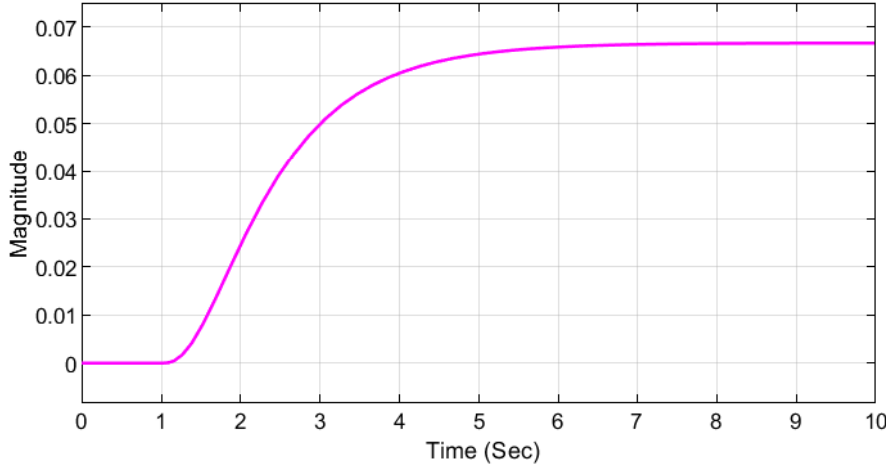


Figure 4.4: Open loop step response of the given system

From the step response, it is clearly seen that the output response does not follow the desired response, which is the step response. So, in order to get the desired response, a controller is needed.

Now for the unity negative feedback system, the characteristics equation is given as:

$$q(s) = 1 + G(s)H(s)$$

$$q(s) = 1 + \frac{K}{(s+1)(s+3)(s+5)}$$

$$q(s) = s^3 + 9s^2 + 23s + (15 + K) = 0$$

Using this characteristics equation, draw R-H table

Table 4.3: R-H table

s^3	1	23
s^2	9	(15+K)
s^1	$\frac{207-(15+K)}{9}$	0
s^0	15+K	

For stability, the coefficients of s^1 and s^0 must be positive. So with these condition, we find the range for stability and it is given as:

4.1 Controller Design By Ziegler-Nichols Tuning Method

$$-15 < K < 192$$

In order to have sustained oscillation, the value of gain K should be maximum i.e,

$$K = K_{max} = K_{cr} = 192$$

With this critical gain, there will be sustained oscillation which frequency can be found from the auxiliary equation,

$$9s^2 + (15 + 192) = 0$$

$$s = j4.8$$

That mean frequency of oscillation (ω_{cr}) will be 4.8 rad/s

With this frequency of oscillation, we can find out the critical time period and it is given as,

$$P_{cr} = \frac{2 * \pi}{\omega_{cr}}$$

$$P_{cr} = 1.31sec$$

Now with the help of Table 4.1 we can find parameters of the PID controller as follows:

$$K_p = 0.6 * K_{cr} = 86.4$$

$$T_i = \frac{K_p}{K_I} = 0.5 * P_{cr}$$

$$\frac{K_p}{K_I} = 0.5 * 1.31$$

4. Controller Design and Close Loop Simulation of BLDC Motor

$$K_I = 175.87$$

$$T_D = \frac{K_D}{K_P} = 0.125 * P_{cr}$$

$$\frac{K_D}{K_P} = 0.125 * 1.31$$

$$K_D = 18.86$$

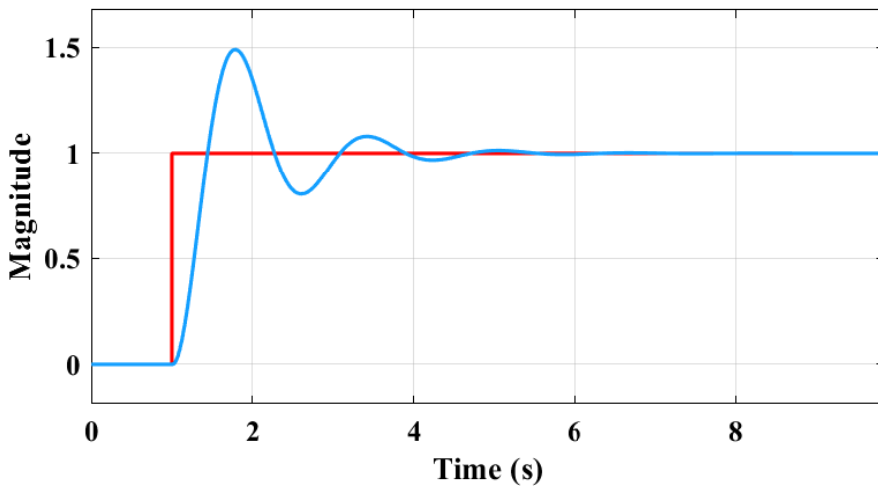


Figure 4.5: Close loop step response for the given system

From the above analysis, it was observed that with the derived value of parameters of the PID controller, we got stable and desired close loop step response, But the settling time was large.

The BLDC motor also got a stable and desired response, but again, the settling time was quite high, which is not good for the motor because the motor has to respond quickly to changes.

4.2 Close Loop Control of BLDC Motor

In order to control the behaviour of a Brushless DC (BLDC) motor, closed-loop simulation requires the integration of a feedback control system. Typically, the feedback mechanism consists of sensors that detect the position or speed of the motor, a controller that processes the data, and an actuator that modifies the motor inputs as necessary.

With closed-loop operation, the drive can run at any speed that is required. When using closed-loop operation, the reference speed can be adjusted at any moment to ensure that the drive is operating at the appropriate speed. In open loop control, the speed is fixed to this reference value. The actual motor speed is supplied back into the input in a closed-loop speed control drive. This speed can be adjusted and increased to the required pace with the use of an appropriate control system. An error signal is produced when the reference speed value is used to measure the actual speed and feeds it back into the input [15].

We are going to discuss the following three close-loop control techniques:

- DC control technique
- Field-oriented control technique
- Hysteresis current control technique

4.2.1 DC Control Technique

In this control technique, We are controlling the speed of the BLDC Motor by taking the DC side current as reference. Thus, unlike other ac quantity control techniques, this one does not require the conversion from ABC-DQ, and it also uses fewer controllers overall.

First we will sense the speed and compare it to the reference speed and will generate the error signal. A PI controller receives this error and uses an appropriate proportional and integral gain value to control the speed. Both the previous and current errors are eliminated by this PI controller. When speed is fed through a PI controller, the current value is referenced. The reference current is generated by the error signal that is created when real speed is measured using reference speed. The reference current is measured using

4. Controller Design and Close Loop Simulation of BLDC Motor

the actual stator current once more, and the error that is produced is sent to the current controller. To turn the voltage source inverter (VSI) switches ON or OFF, the current controller generates gate pulses [16]. The stator currents to the BLDC motor are managed by the appropriate switching operation, which also controls the VSI.

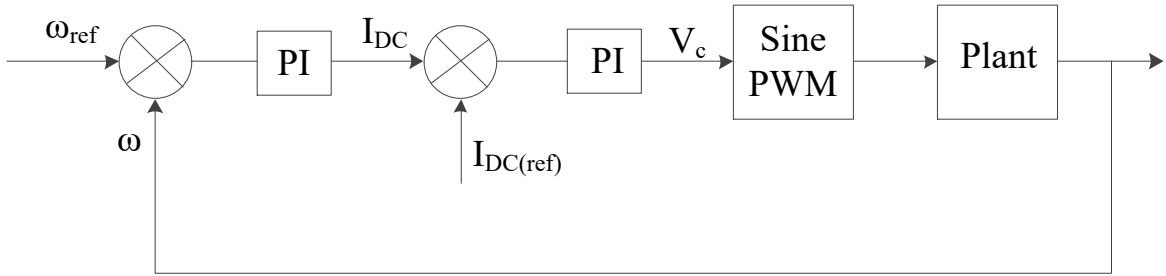


Figure 4.6: Block diagram of DC control technique

In order to design the controller, we need a plant transfer function. In our case, BLDC motor is the plant. So, the transfer function of the BLDC motor can be found with the help of characteristics equations.

The characteristic equations of the BLDC motors can be represented as:

$$v_{as}(t) = L \frac{di(t)}{dt} + R_s \cdot i(t) + e_{as}(t) \quad (4.2)$$

$$e_{as}(t) = K_b \cdot \omega(t) \quad (4.3)$$

$$T(t) = K_t \cdot i(t) \quad (4.4)$$

$$T(t) = J \frac{d\omega(t)}{dt} + F \cdot \omega(t) \quad (4.5)$$

where,

$v_{as}(t)$ = voltage supplied to the phase a of the stator winding, $\omega(t)$ = motor speed, L = inductance of the stator, $i(t)$ = current of the circuit, R_s = resistance of the stator, $e_{as}(t)$ = back emf, T = torque of motor, F = viscous coefficient, J = moment of inertia, K_t = motor torque constant, and K_b = back emf constant [17].

Taking the laplace transform of all characteristics equations, we get

$$V_{as}(s) = Ls * I(s) + R_s \cdot I(s) + E_{as}(s) \quad (4.6)$$

$$E_{as}(s) = K_b \cdot \omega(s) \quad (4.7)$$

$$T(s) = K_t \cdot I(s) \quad (4.8)$$

$$T(s) = Js * \omega(s) + F \cdot \omega(s) \quad (4.9)$$

4.2.2 Controller design For Speed Loop

Since the input to the speed loop PI controller is the speed and the output is the current. So the plant transfer function for this controller will be $\frac{\omega(s)}{I(s)}$. from equation 4.8

$$T(s) = Js * \omega(s) + F \cdot \omega(s) \quad (4.10)$$

putting the value of T(s) from equation 4.7 in the above equation we get,

$$k_t * I(s) = (Js + F) * \omega(s)$$

$$\frac{\omega(s)}{I(s)} = \frac{k_t}{Js + F} \quad (4.11)$$

We get the desired plant transfer function for the speed loop by putting all the given value,

$$\frac{\omega(s)}{I(s)} = \frac{0.668}{0.008s + 1 * 10^{-3}}$$

Now by using the "k-factor method for controller design" technique, we get the parameter of PID controller i.e the value of K_p , K_I and K_D as follow:

- $K_P = 3.084$
- $K_I = 0.308$

4. Controller Design and Close Loop Simulation of BLDC Motor

4.2.3 Controller design For Current Loop

Since the input to the current loop PI controller is, the current and the output is the duty. So the plant transfer function for this controller will be $\frac{I(s)}{m(s)}$.
from equation 4.5

$$V_{as}(s) = Ls * I(s) + R_s.I(s) + E_{as}(s)$$

Putting the value of $E_{as}(s)$ from equation 4.6 we get,

$$V_{as}(s) = Ls * I(s) + R_s.I(s) + K_b.\omega(s) \quad (4.12)$$

From equation 4.8 we know that,

$$T(s) = Js * \omega(s) + F.\omega(s) \quad (4.13)$$

Putting the value of $T(s)$ from equation 4.7 in above equation we get,

$$k_t * I(s) = Js * \omega(s) + F.\omega(s)$$

or,

$$\omega(s) = \frac{k_t * I(s)}{Js + F}$$

Putting the value of $\omega(s)$ in equation 4.10 we get,

$$V_{as}(s) = Ls * I(s) + R_s.I(s) + \frac{k_t k_b}{Js + F} I(s) \quad (4.14)$$

For 3-ph Inverter operating in sine PWM we know that,

$$v_o(L - L) = \sqrt{3}m \frac{V_{DC}}{2} \sin\omega t$$

or,

$$v_o(ph) = m \frac{V_{DC}}{2} \sin\omega t$$

or,

$$v_o(ph)_r = m \frac{V_{DC}}{2\sqrt{2}}$$

Now putting this value in equation 4.14 we get,

$$m \frac{V_{DC}}{2\sqrt{2}} = I(s)(Ls + R_s + \frac{k_t k_b}{Js + F})$$

After solving this equation we get,

$$\frac{I(s)}{m(s)} = \frac{V_{DC}(Js + F)}{2\sqrt{2}[LJs^2 + (LF + RJ)s + (RF + k_b k_t)]} \quad (4.15)$$

We get the desired plant transfer function for current loop by putting all the given value,

$$\frac{I(s)}{m(s)} = \frac{0.4s + 0.05}{1.131 * 10^{-5}s^2 + 0.0339s + 132.26}$$

Now by using "k-factor method for controller design" technique, we get the parameter of PI controller i.e value of K_p and K_I as follow:

- $K_P = 0.702$

- $K_I = 766$

4. Controller Design and Close Loop Simulation of BLDC Motor

4.2.4 Simulation Diagram for DC Current Control (DCC) Technique

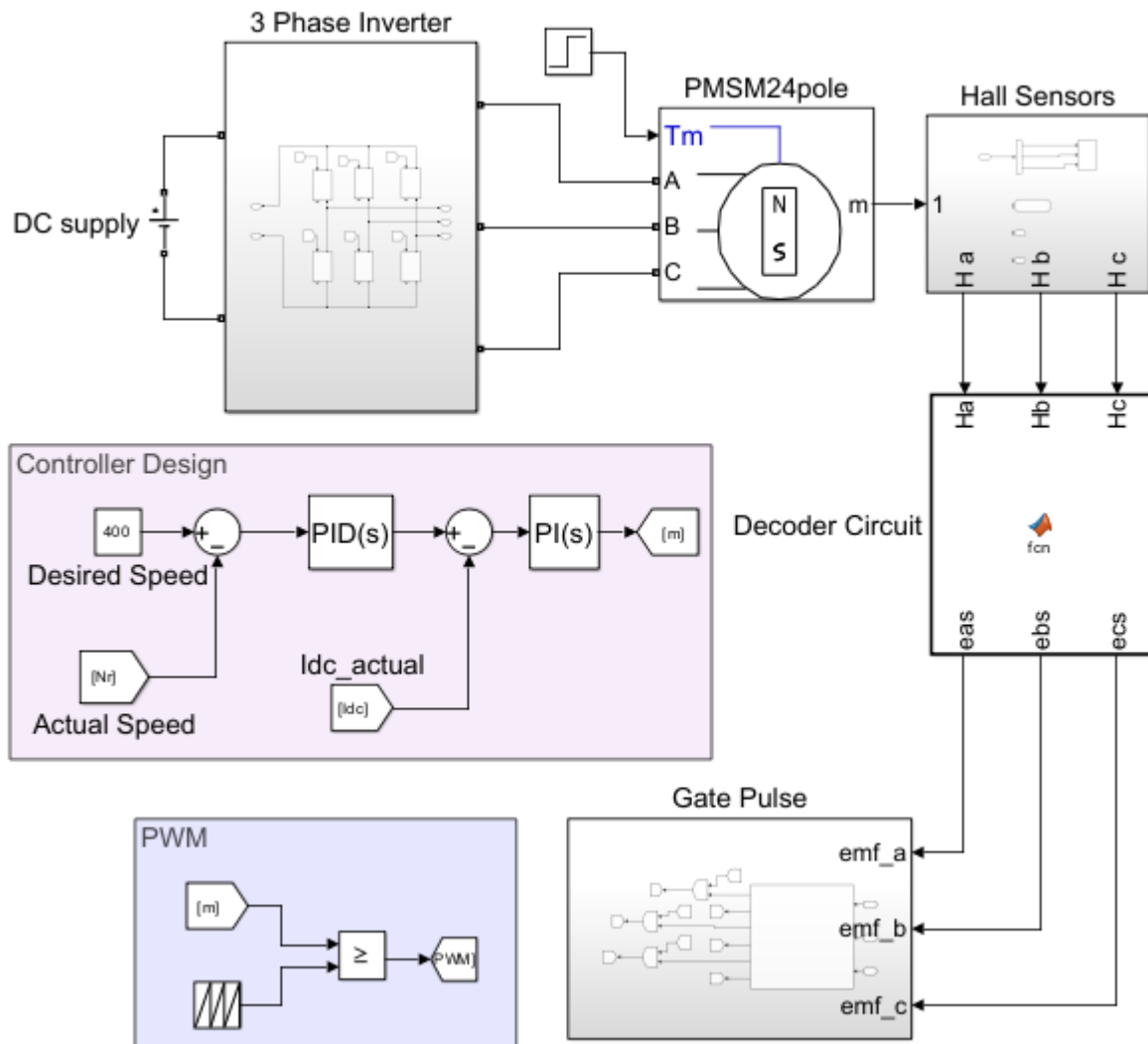


Figure 4.7: Block diagram of DC control technique

4.2.5 Simulation Results

- For Desired Speed of 400 rpm

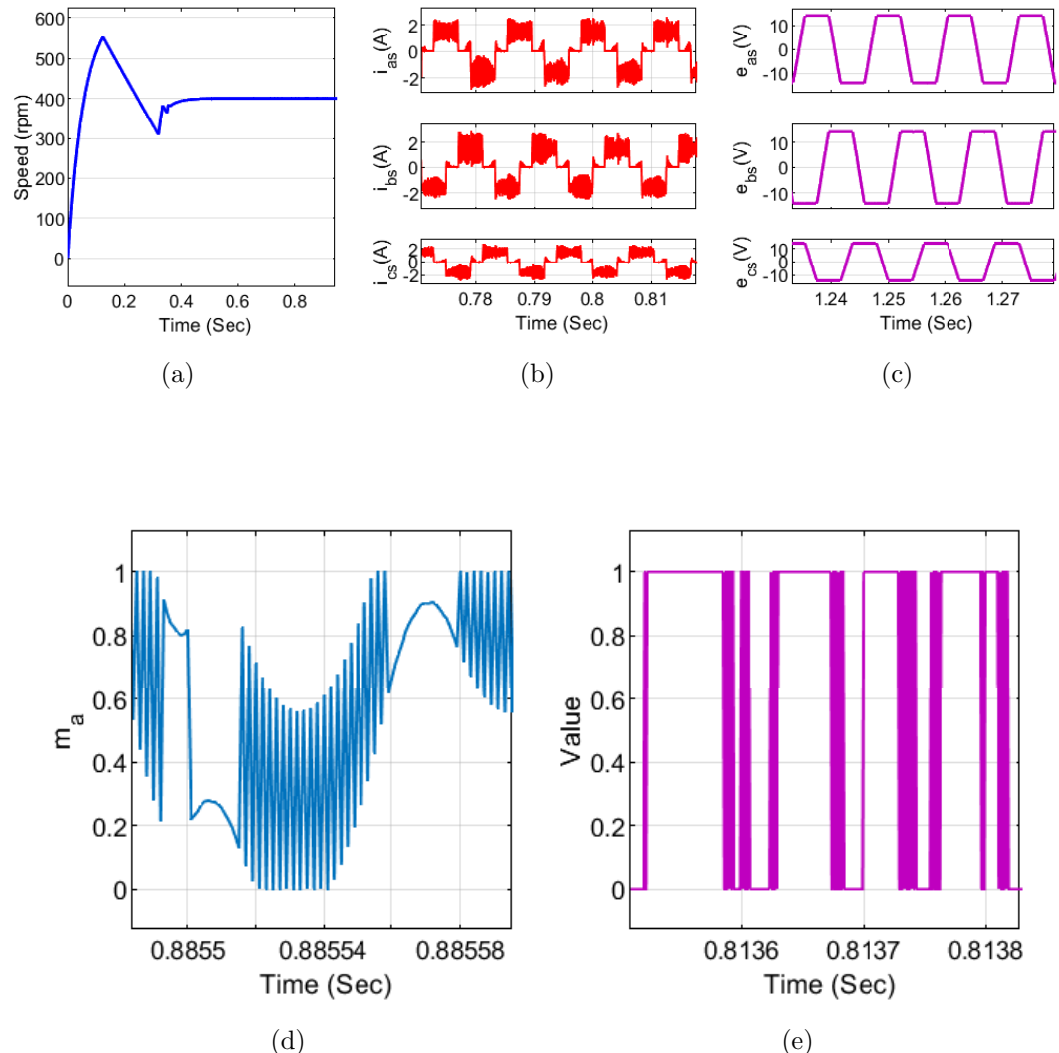


Figure 4.8: Waveform at 400 rpm: (a) rotor speed (b) stator current (c) back emf (d) modulating signal (e) switching pulses

4. Controller Design and Close Loop Simulation of BLDC Motor

4.2.6 Field Oriented Control (FOC) Technique

Vector control is another name for field-oriented control, or FOC. It was first created for variable frequency motor drives, which use vector control of voltages and currents to align electromagnetic fields in space. The idea behind the variable voltage and frequency approach is to adjust the input voltage and frequency to control the rotor speed and torque. The fundamental limitation of sinusoidal commutation is the regulation of time-varying motor currents, which lead to a breakdown at higher speeds and frequencies because of the proportional and integral (PI) controllers' narrow bandwidth. This issue is resolved by FOC by directly regulating the current space vector in the rotor's d,q reference frame [18].

Motor voltages and currents are adjusted using Field Oriented Control within the rotor's d-q reference frame. Because of this, measurable motor currents need to be mathematically converted from the three-phase static reference frame of the stator windings to the two-axis rotating d-q reference frame before they can be processed by the PI controllers. Similar to this, before the voltages can be used for PWM output, they must be converted from the dq frame of the rotor to the three-phase reference frame of the stator. These changes typically call for a DSP or high-performance processor, which is the foundation of field-oriented control, to have quick math capabilities. Fig. 4.9 illustrates the Block diagram of the proposed field-oriented control(FOC) scheme of a BLDC motor.

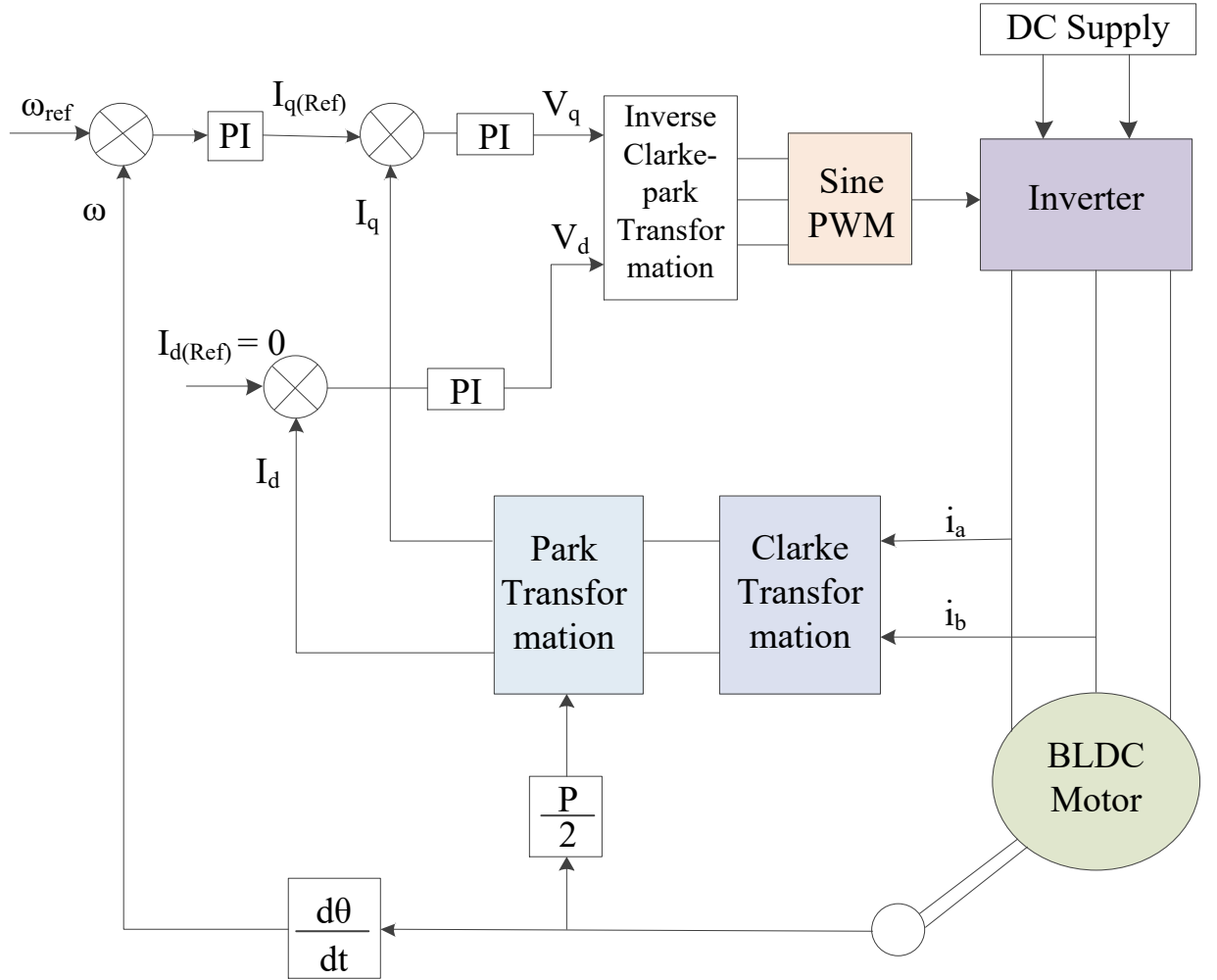


Figure 4.9: Block diagram of proposed field oriented control scheme

The reference frame transformations are best explained as a two-part procedure, even if they can be completed in one step. The motor currents are first converted to a fixed orthogonal reference frame from the 120 degree physical frame of the motor stator windings. Next, they are translated to the rotor's spinning frame from the stator's fixed frame. For the direct current component and the quadrature current component, two P-I controllers are employed [19].

There is zero input into the direct current controller. As a result, the current space vector is forced to point only in the quadrature direction, driving the direct current component to zero. By producing useable torque only through quadrature current, the system's torque

4. Controller Design and Close Loop Simulation of BLDC Motor

efficiency is maximised. Using quadrature current, the second P-I controller receives the requested torque as input. As a result, the desired torque is tracked by the quadrature current.

A voltage space vector with respect to the rotor is represented by the outputs from the two P-I controllers. These static signals are subjected to a sequence of reference frame transformations that yield voltage control signals for the output bridge, mirroring the transformation applied to motor currents. They are then converted from the rotor's revolving d-q frame to the stator's fixed x-y frame. The voltage signals are then transformed from an orthogonal frame to the physical frame of the U, V, and W motor windings, which is 120 degree [20]. This results in three voltage signals appropriate for control of the PWM output modulator.

Now by using the "Ziegler-Nichols method for controller design" technique, we find the controller's parameter for different loops:

- For speed loop

Values of K_p , K_I and K_D are as follows: $K_P = 3.08$ and $K_I = 0.308$

- For current loop

Values of K_p and K_I are as follows: $K_P = 0.702$ and $K_I = 766$

4.2.7 Simulation Diagram for Field Oriented Control (FOC) technique

A voltage space vector with respect to the rotor is represented by the outputs from the two P-I controllers. These static signals are subjected to a sequence of reference frame transformations that yield voltage control signals for the output bridge, mirroring the transformation applied to motor currents. They are then converted from the rotor's revolving d-q frame to the stator's fixed x-y frame. Following that, the voltage signals are transformed from an orthogonal frame to the physical frame of the U, V, and W motor windings.

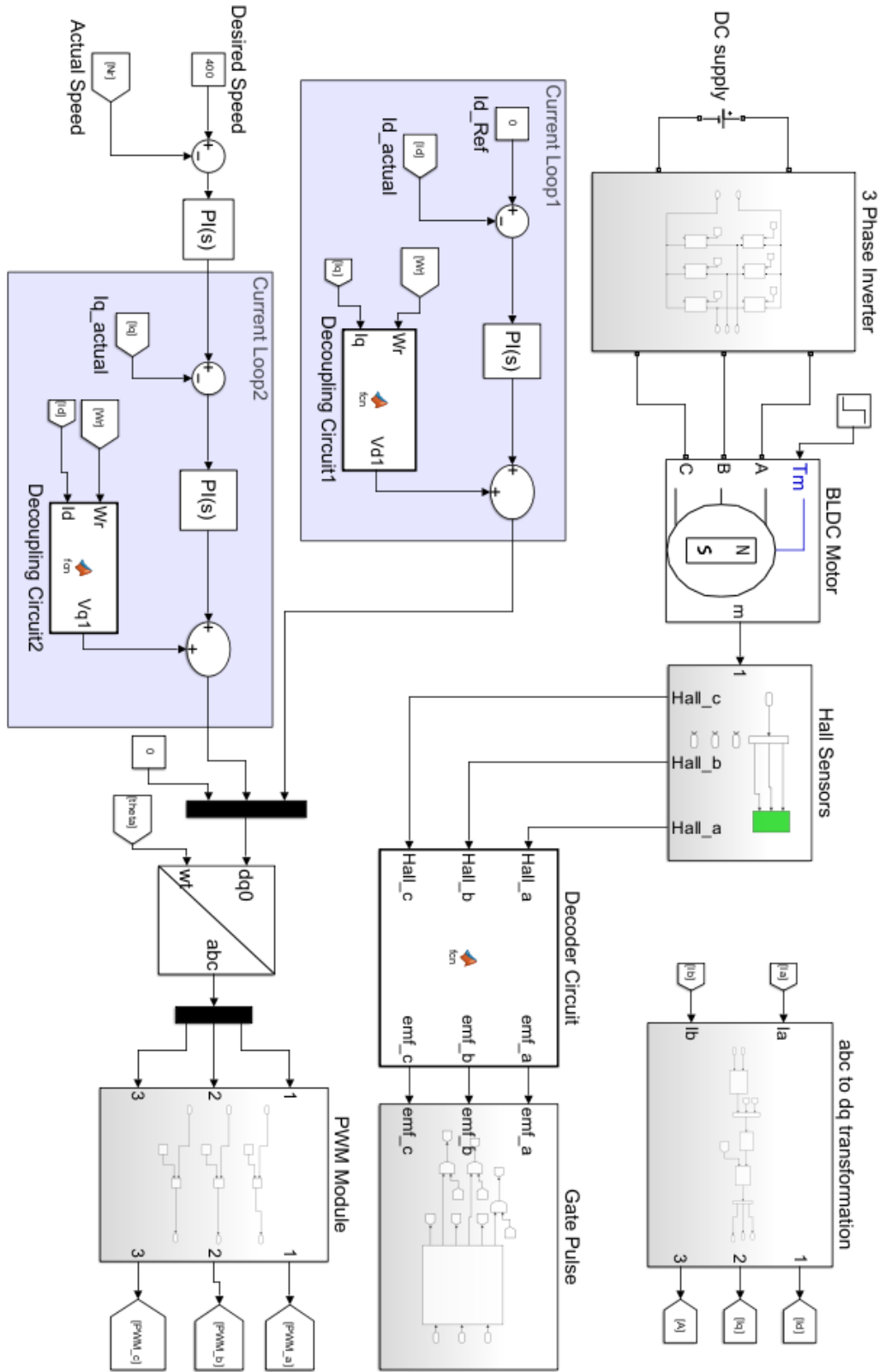


Figure 4.10: Close loop simulation diagram for 180° commutation

4. Controller Design and Close Loop Simulation of BLDC Motor

4.2.8 Simulation Results for 120° conduction

Here we are using field oriented control (FOC) technique to perform the close loop control of BLDC motor in 120° conduction mode.

Here we are going to check whether ripple in speed and stator current is getting reduced or not as compare to open loop simulation.

- For Desired Speed of 400 rpm

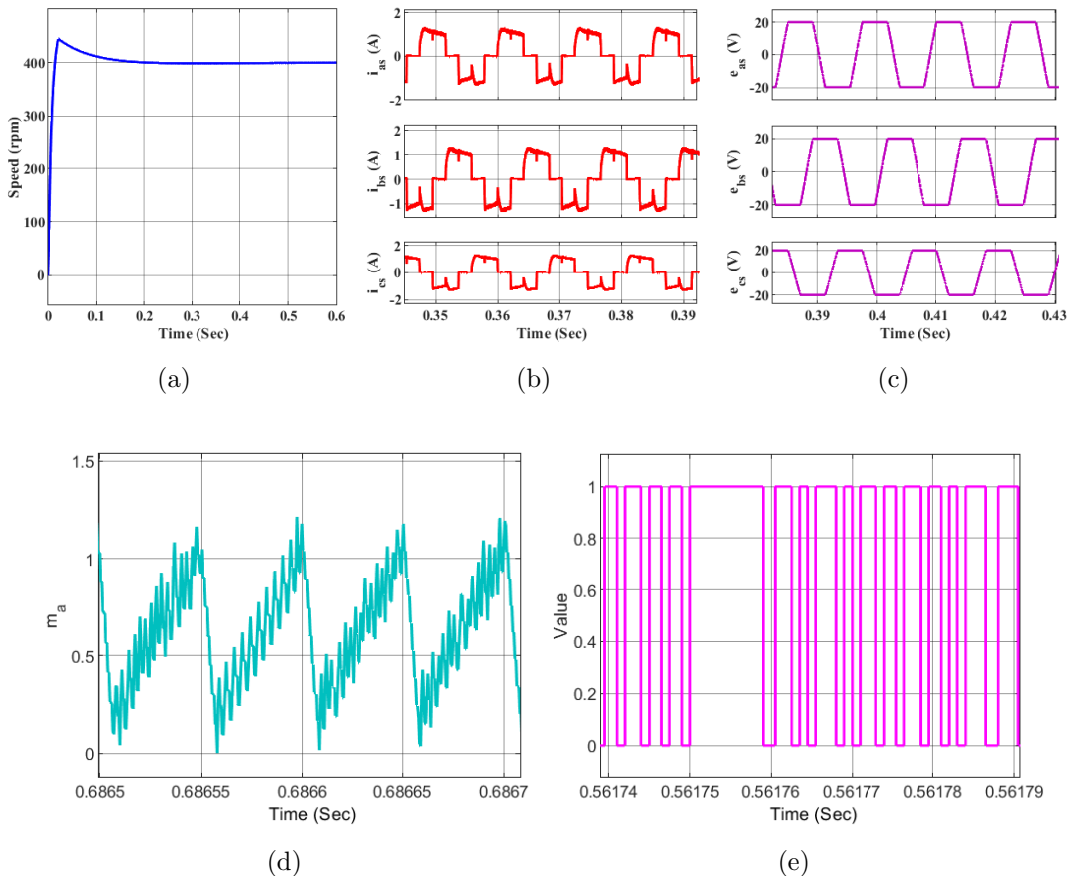


Figure 4.11: Waveform at 400 rpm: (a) rotor speed (b) stator current (c) back emf (d) modulating signal (e) switching pulses

4.2.9 Results

We will vary the all three quantities that is torque, supply voltage and motor speed one by one while keeping other two quantities constant and we will observe the duty ratio in each case.

- Varying The Torque While Keeping Supply Voltage and Speed Constant

Tm (N-m)	Supply voltage	Rotor Speed (rpm)	Duty (D)
1 N-m	50 V	300 rpm	0.421
2 N-m	50 V	300 rpm	0.491
3 N-m	50 V	300 rpm	0.547

- Varying The Supply Voltage While Keeping Torque and Speed Constant

Tm (N-m)	Supply voltage	Rotor Speed (rpm)	Duty (D)
50 V	300 rpm	1 N-m	0.614
30 V	300 rpm	1 N-m	
20 V	300 rpm	1 N-m	

- Varying The Speed While Keeping Supply Voltage and Torque Constant

Rotor Speed (rpm)	Supply voltage (V)	Tm (N-m)	Duty (D)
200 rpm	50 V	1 N-m	0.329
300 rpm	50 V	1 N-m	
450 rpm	50 V	1 N-m	

4.2.10 Hysteresis Current Control Technique

Hysteresis control is the simplest current control scheme. Two control loops are utilised for the BLDC motor's closed-loop control. There is a torque control loop inside and a speed control loop outside. Based on the inverter's control switching action, the hysteresis bandwidth limits are compared to the current errors. The block diagram for the suggested hysteresis current control of a BLDC motor is shown in Figure 3.3.

First, Reference speed is compared to the drives' actual speed, and the resulting error is given to the speed controller. The controlled signal is compared with the actual torque, and an error signal is generated. From this error signal, actual currents are calculated after dividing by the torque constant. This actual current is then compared with the reference current, and the error is given to the hysteresis block where some finite band for hysteresis control is provided [21]. From the hysteresis block, a modulating signal is generated, and these modulating signals are then given to the sine PWM block to generate the desired switching.

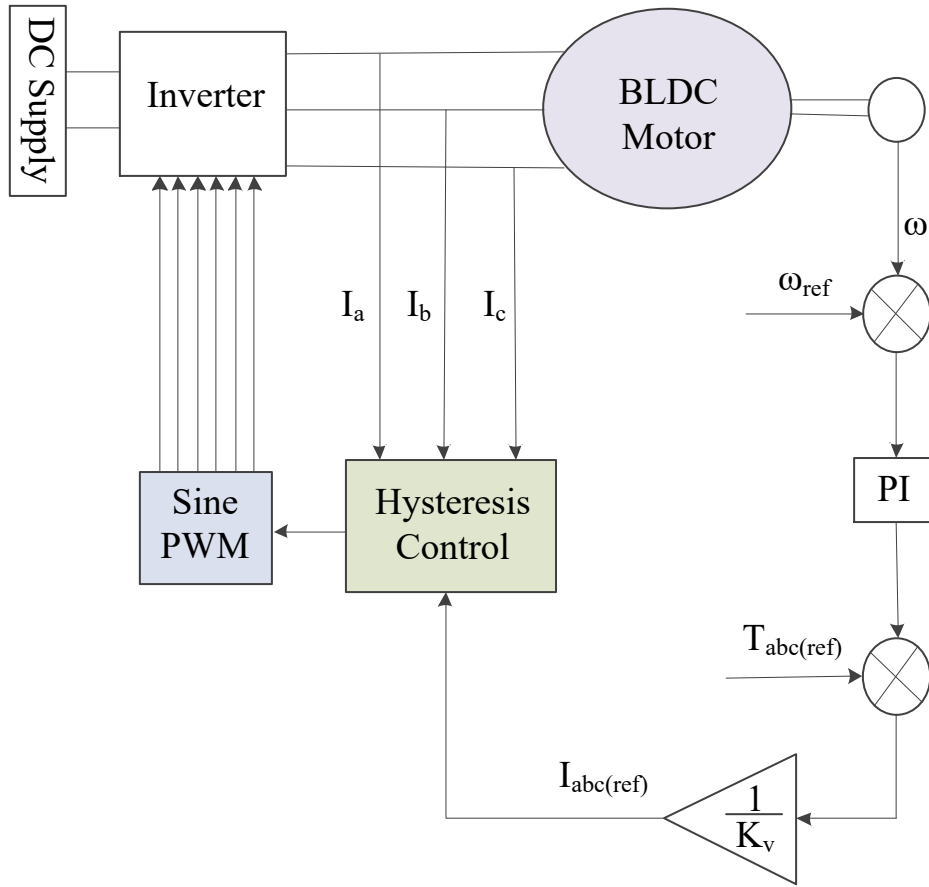


Figure 4.12: Block diagram of hysteresis current control technique

Now by using the "Ziegler-Nichols method for controller design" technique, we get the parameter of PID controller i.e value of K_p , K_I and K_D as follows: $K_P = 188.1193$, $K_I = 11.7575$ and $K_D = 5$

4.2.11 Simulation Diagram for Hysteresis Current Control Technique

Hysteresis control is the simplest current control scheme. Two control loops are utilised for the BLDC motor's closed-loop control. There is a torque control loop inside and a speed control loop outside. Based on the inverter's control switching action, the hysteresis bandwidth limits are compared to the current errors.

4. Controller Design and Close Loop Simulation of BLDC Motor

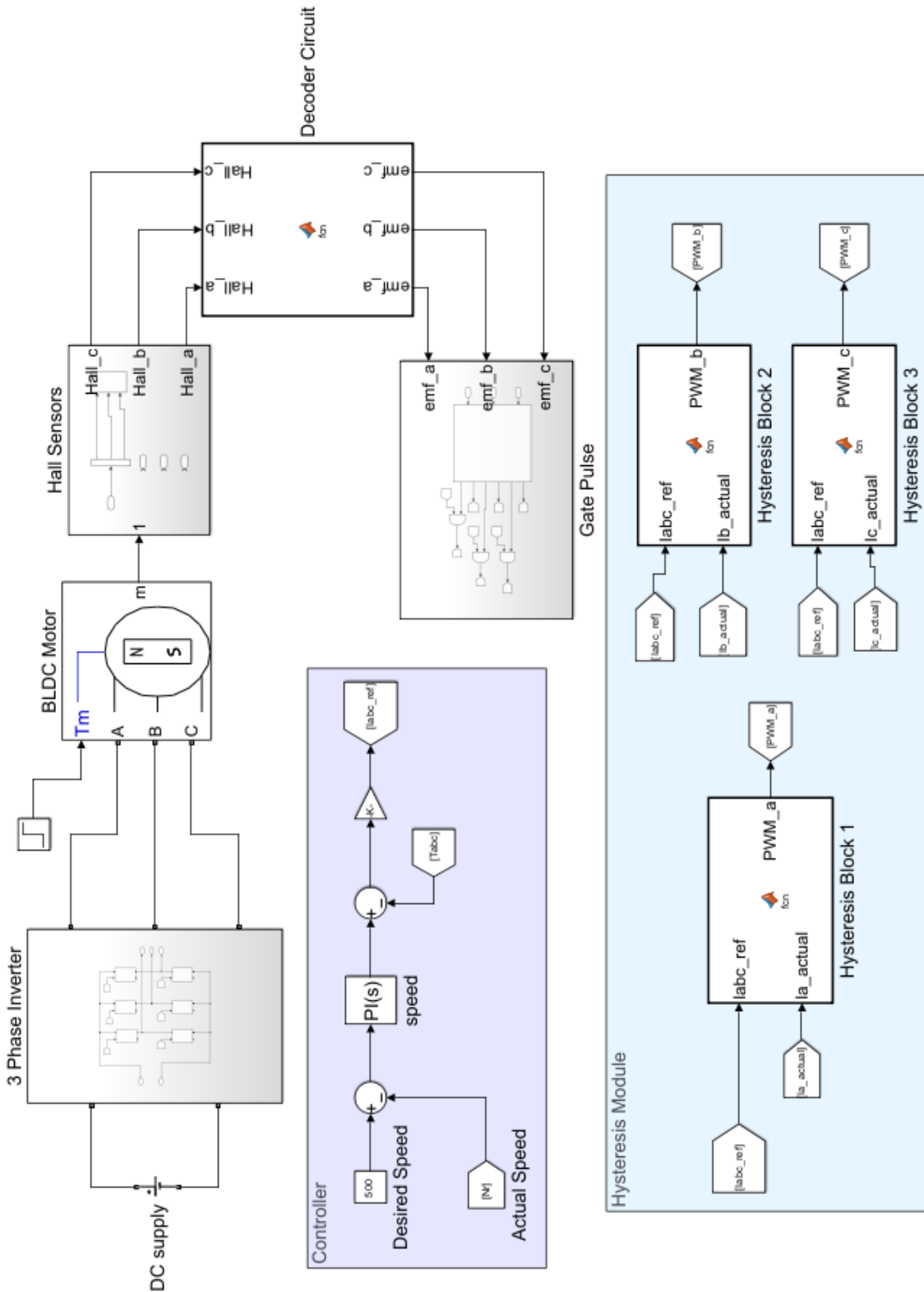


Figure 4.13: Close loop simulation diagram for 180° commutation

4.2.12 Simulation Results for 120° conduction

- For Desired Speed of 400 rpm

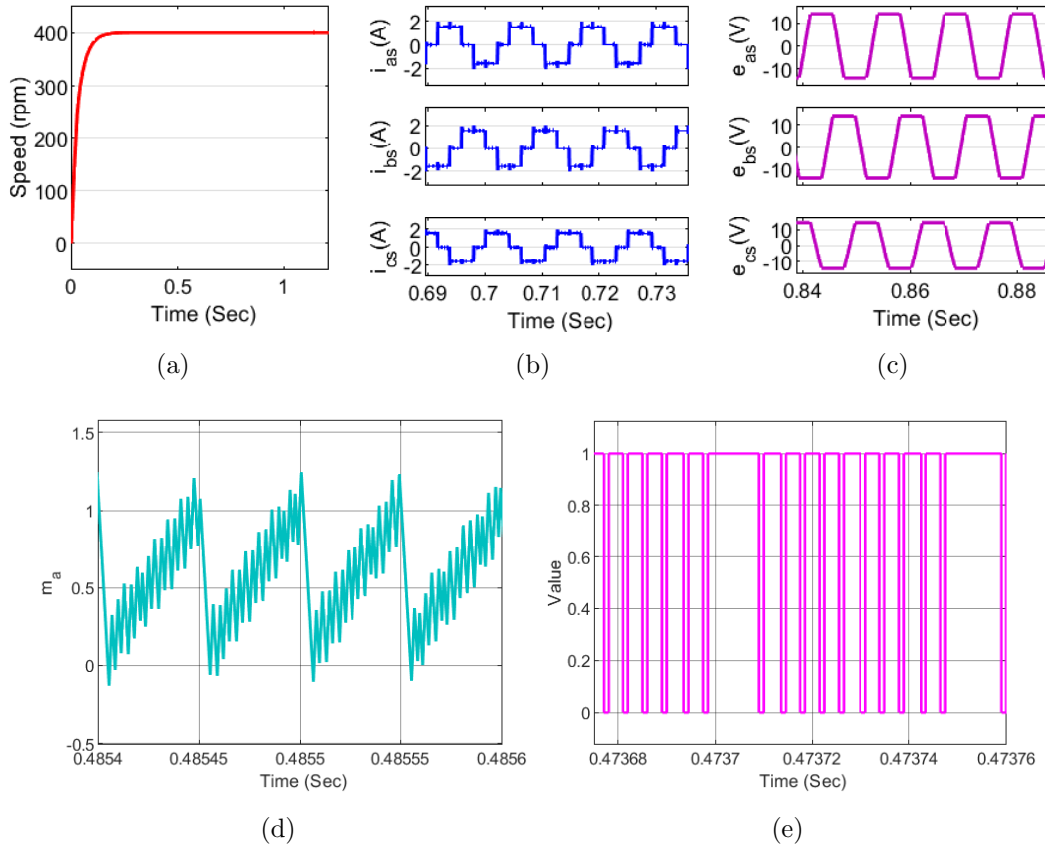


Figure 4.14: Waveform of rotor speed, stator current, back emf, modulating signal and back switching pulses for desired speed of 400 rpm: (a) rotor speed (b) stator current (c) back emf (d) modulating signal (e) switching pulses

4. Controller Design and Close Loop Simulation of BLDC Motor

5

Hardware

Contents

5.1	Introduction	58
5.2	Briefs description of hardware setup	59
5.3	Hardware implemantation	61
5.4	Open loop hardware implementation	66
5.5	Close loop hardware implementation	70

5. Hardware

5.1 Introduction

Hardware implementation of BLDC motor speed control is done using Waijung Blockset and STM32F4 DISCOVERY board.

Waijung is a Simulink Blockset that can be used to easily and automatically generate C code from Matlab/Simulink simulation models for many kinds of microcontrollers (Targets). The Waijung block in Matlab Simulink models are automatically converted into C language followed by assembly language code and loaded into the microcontroller memory. This enables the user to directly use various predefined blocks in Matlab Waijung blocks to generate the signals and completely eliminate the coding requirement [22].

The STM32F407G-DISCOVERY board developed by STM is used as a microcontroller in the setup. The development boards are programmed using Waijung Block sets seen in Fig. 5.1 regarding practicality and stable operation. The software created with the block sets is embedded in the STM32F407G-DISCOVERY board with the Code-Generation tool [23].

STMicroelectronics STM32F407G is an ARM Cortex M4 32-bit microcontroller (MC) targeted for high-efficiency digital processing with rich peripherals. It has the capability to process 210 million instructions per second and can perform a single cycle multiplication and accumulation. Some important features of this microcontroller are:

- 1MB of Flash memory, 192 KB of RAM in an LQFP100 package running at 168 MHz (max), providing peak throughput of 210 MIPs.
- On-board ST-LINK/V2 debugger for hardware level debugging (SWD connector for programming and debugging)
- 3×12 -bit, 2.4 million samples per second A/D converters: up to 24 channels (simultaneous sampling of all three ADCs is possible)
- 2×12 -bit D/A converters
- General-purpose direct memory access (DMA): 16-stream DMA controller with FIFOs and burst support.

5.2 Briefs description of hardware setup

- Up to 17 timers: up to twelve 16-bit and two 32-bit timers up to 168MHz, each with up to 4 IC/OC/PWM or pulse counter and quadrature (incremental) encoder input.
- 6 complimentary PWM channels with programmable dead time insertion.
- Up to 140 general purpose input and outputs (GPIOs).
- Board power supply: through USB bus or from an external 5 V supply voltage [24].

Due to lower cost and highly simplified programming, an ARM Cortex 32-bit M4 microcontroller is selected as the controller board.

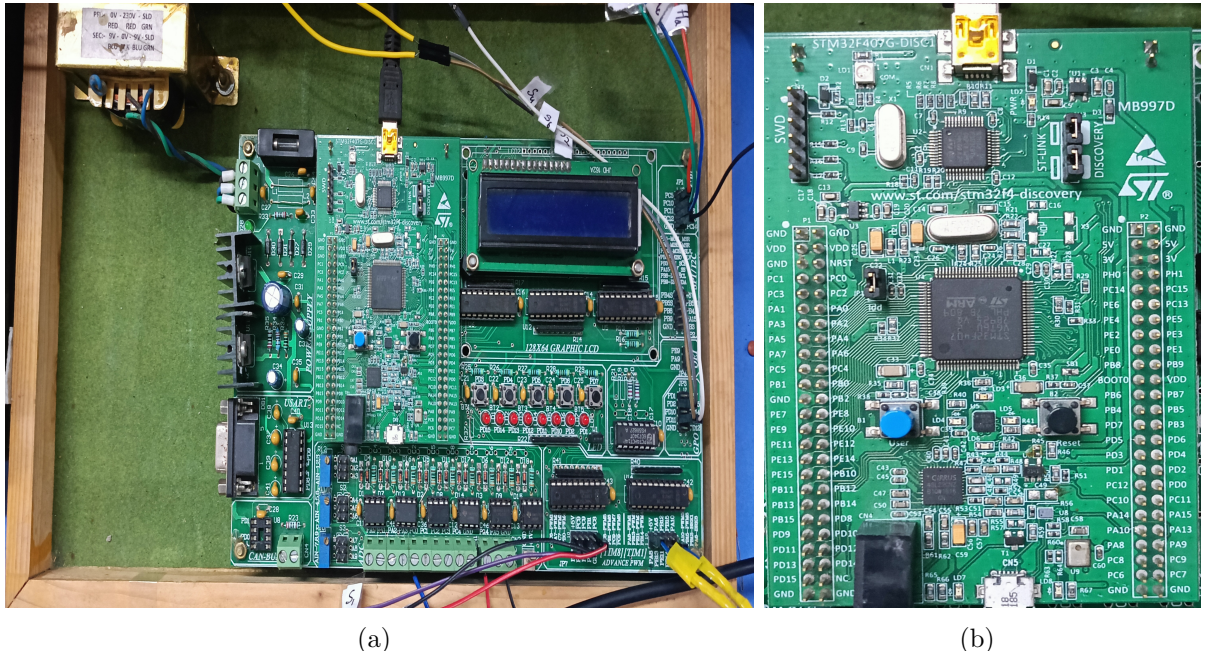


Figure 5.1: (a) Motherboard which include STM32F4 discovery board (b) STM32F407G-DISCOVERY board

5.2 Briefs description of hardware setup

For the motor drive application, IGBT Modules 6MBI100S-120 developed by Fuji Electric have been used, which contain six IGBT switches rated at 1200V/100A. A decoder circuit was constructed to first receive the Hall signals from the motor. After passing through the NAND gate, these signals were sent to the microcontroller. The decoder circuit then received the six switching pulses generated by the microcontroller.

5. Hardware

The driver circuits mounted on the decoder circuit receive signals from the microcontroller, which shares a common ground for negative group switches (S_2 , S_6 and S_4) and have separate ground for positive group switches (S_1 , S_3 and S_5). These non-isolated signals are used to produce the six isolated gate signals required to drive the switches. Additionally, the circuit contains various protection mechanisms. The starter kit consists of two boards: a daughter board containing ST Discovery card for STM32F407VGT6 microcontroller and a mother board with provisions to provide buffering and signal conditioning of various signals [23]. This board contains the following peripherals: 8 buffered digital inputs (jumper (JP)-1), 8 buffered digital outputs (JP-2), 4 High speed buffered outputs, 2 High speed buffered inputs (JP-3), 6 Buffered PWM channels with break signal, Quadrature Encoder Interface (QEI) inputs (A,B,Z) (JP-6), 5 pushbutton keys, 16 x 2 LCD, 2 DAC channels and 9 Buffered analog inputs channels with low pass filter and overvoltage protection diodes. The sensor cards are used to sense various voltage and current signals and provide the feedback signals required for the closed-loop operation of the PE circuits.

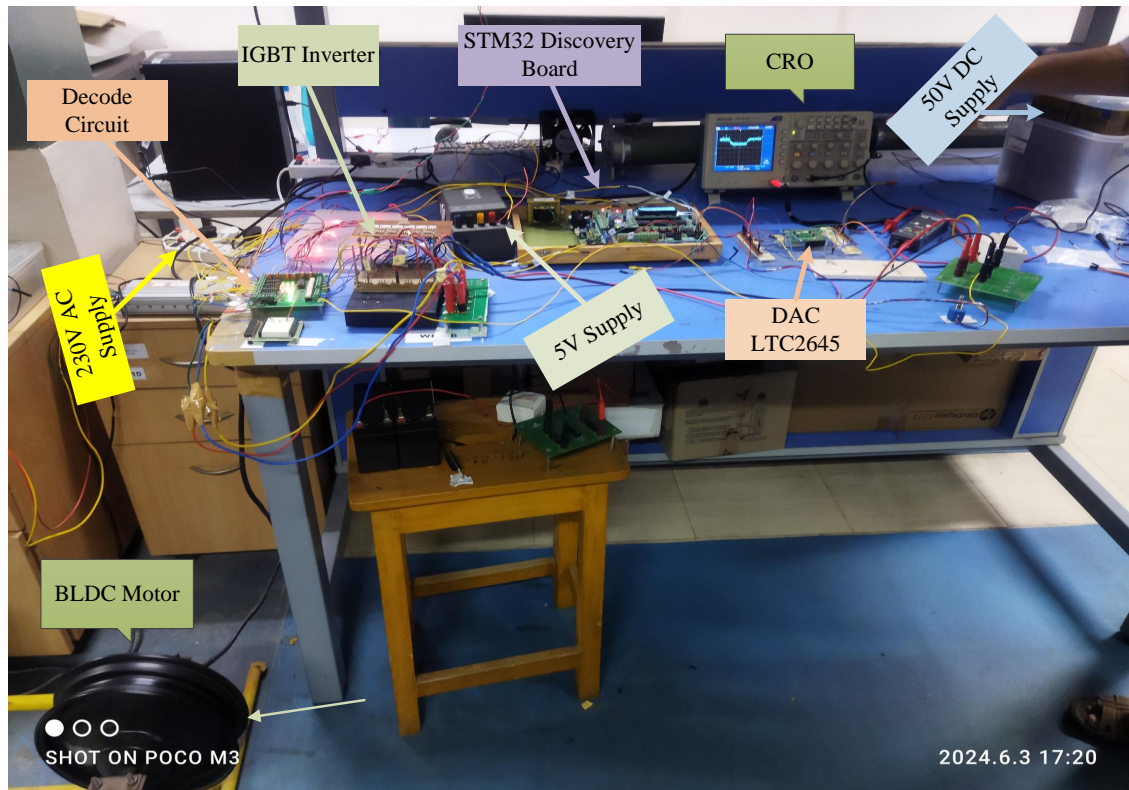


Figure 5.2: Hardware Set up

5.3 Hardware implementation

This subsection presents the steps required to develop a model in MATLAB for the microcontroller unit and the corresponding hardware setup for validation. To develop a program, open a new file in MATLAB/Simulink and save it. Various models can be developed using the predefined blocks in the Waijung Blockset. These predefined blocks can be directly converted into C code for any microcontroller unit. This simplifies the process of developing a model to generate gate/firing pulses and eliminates the need for C/assembly language coding. To develop any model using the MATLAB/Simulink Waijung Blockset, simply drag and drop the predefined blocks from the Waijung library. Any PE converter model must contain the following three fundamental blocks:

a) Target setup block: It defines the compiler, microcontroller unit, base sampling time, etc. This setup will be the same for any model developed for the given microcontroller unit. To add this block, navigate to the following location in the library: Waijung BlockSet/STM32F407VG Target/Device Configuration, and click and drag the Target Setup block. In the following description, the STM32F407VG microcontroller unit, along with the MDK-ARM compiler and ST-Link programmer or debugger for PE lab experiments, is considered. Set the appropriate options in the dialogue box of the Target Setup block using the pull-down menu.

b) Control Logic blocks: Control logic blocks or code can be developed for any customisable applications using MATLAB/Simulink blocks, such as the pulse generator block, sine generator block, etc. These blocks define the control logic of a model and are used to generate the control signals/firing pulses required for any application [23].

c) Input/output blocks: The predefined Input/output blocks available in the Waijung blocks are used to send the generated control signals to the desired GPIOs for onward transmission to the driver circuit. To add this/these block/s the following location in the library is to be opened: Waijung BlockSet/STM32F407VG Target/On-chip peripherals and click and drag the required block/s.

5. Hardware

The ADC and DAC can be used to design control blocks for closed-loop applications. Waijung BlockSet also contains a pulse width modulation (PWM) block, advanced PWM block, timer block, etc., for developing complex models. Discrete model solver is to be selected from the model configuration parameter in Matlab/Simulink.

Now the model is ready to be loaded into the microcontroller. To load a model, the target first needs to be connected. For that, open the STM32 ST-Link utility software and click on the "Connect Target" option; this will connect the target controller with the Waijung model. To load the code to the controller, use the build command. Click on the "Build Model" symbol or press Ctrl + B in the waijung model; this will upload the code to the controller. The building process consists of the following steps: i) Compiling and ii) Building, which includes generating source code, packing source code, compiling source code, connecting to the target, performing a full chip erase, downloading and verifying, and running the target. These steps are automatically executed once the build command is used. After successful completion of these steps, the corresponding assembly language code is loaded into the microcontroller [22]. This completes the gate signal generation process. These gate signals are collected at the configured GPIO pins and transferred to the power card through jumpers. The switches in the power card are then connected appropriately to obtain a specific PE circuit.

Fig. 5.3 represents the overall block diagram of the operation of a BLDC motor in open loop. First, the three Hall signals were taken from the BLDC motor and given to the NAND gate of the decoder circuit, which was used to provide buffering. These three Hall sensor signals were then given to the microcontroller. Using the input GPIO pins, these three Hall sensor signals were fed into the Waijung simulation model where the commutation logic was written, generating the switching pulses. Then, using the output GPIO pins, these generated pulses were sent from the microcontroller to the decoder circuit.

Now, with the help of gate driver circuits, these generated switching pulses were given to the three-phase inverter, which then supplied power to the BLDC motor.

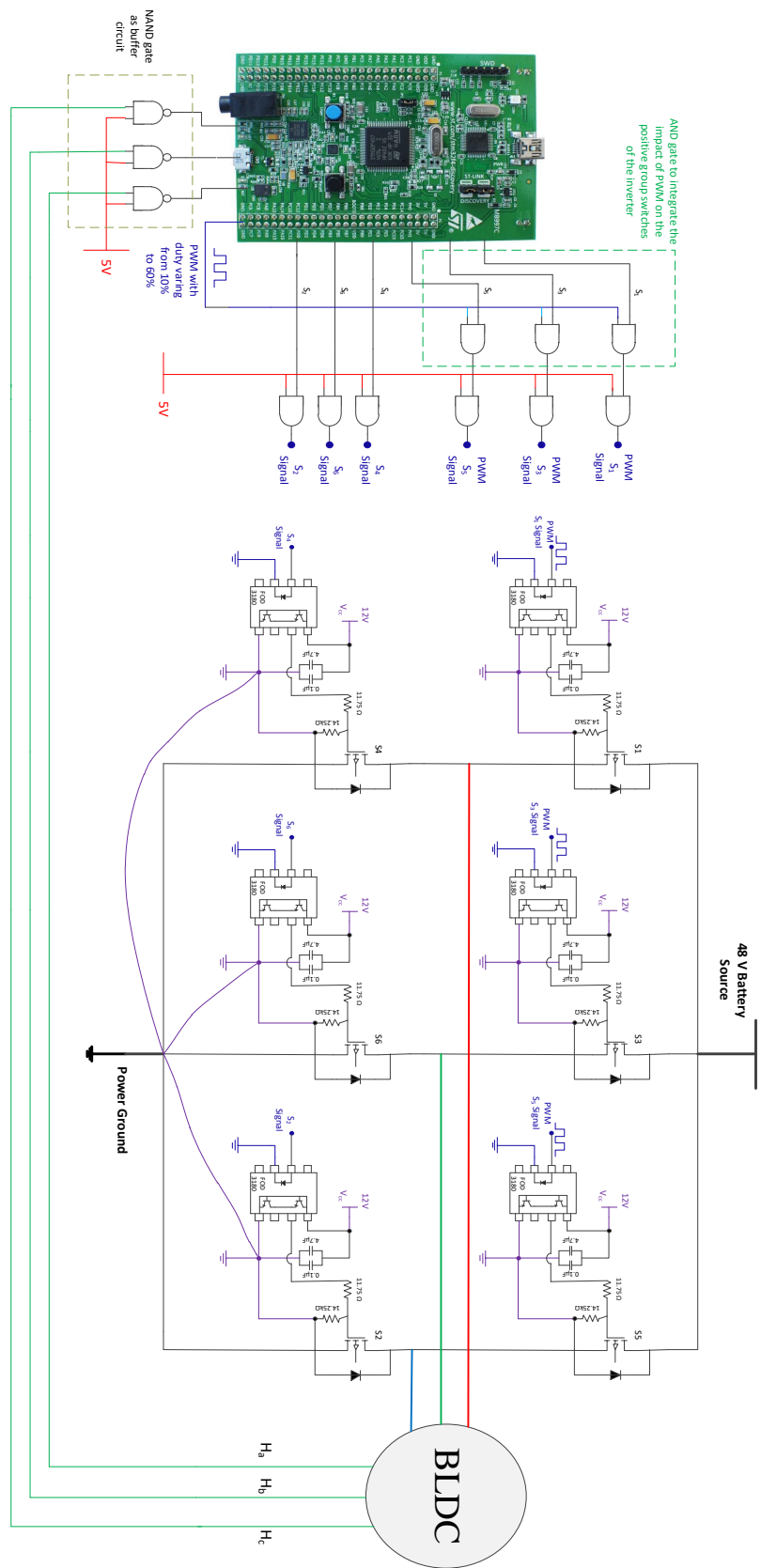


Figure 5.3: Overall Block Diagram Representation

5. Hardware

5.3.1 Decoder Circuit

The decoder circuit used in this project is responsible for receiving signals from the Hall sensors of the BLDC motor and generating six switching pulses, which are then supplied to the three-phase inverter.

Fig. 5.4 represents the decode circuit, which operates in four stages:

In the first stage, the hall sensor from the BLDC motor is taken as input and then passed to the NAND gate for buffering operation. The output of the NAND gate is then sent to the microcontroller.

The decoder circuit used in this project has PWM operation in the second stage. However, since we already performed the PWM action in the Waijung simulation model, this stage needed to be bypassed. To achieve this, an active high signal was given to all NAND gates, causing them to act as buffers.

In the third stage, all six switching pulses (both PWM pulses and regular pulses) are passed through an AND gate, with one terminal connected to an active high supply, making it a buffer circuit. This circuit was implemented to provide protection.

The switching pulses coming from the microcontroller are control signals with low voltage that cannot drive power MOSFETs/IGBTs. Therefore, we require a gate driver circuit that converts these control signals to power signals while maintaining separation between these two types of signals. For this purpose, we used the FOD3180 optocoupler gate driver. Stage four contains six gate driver circuits, which receive all six switching pulses and generate power signals to drive the power MOSFETs/IGBTs.

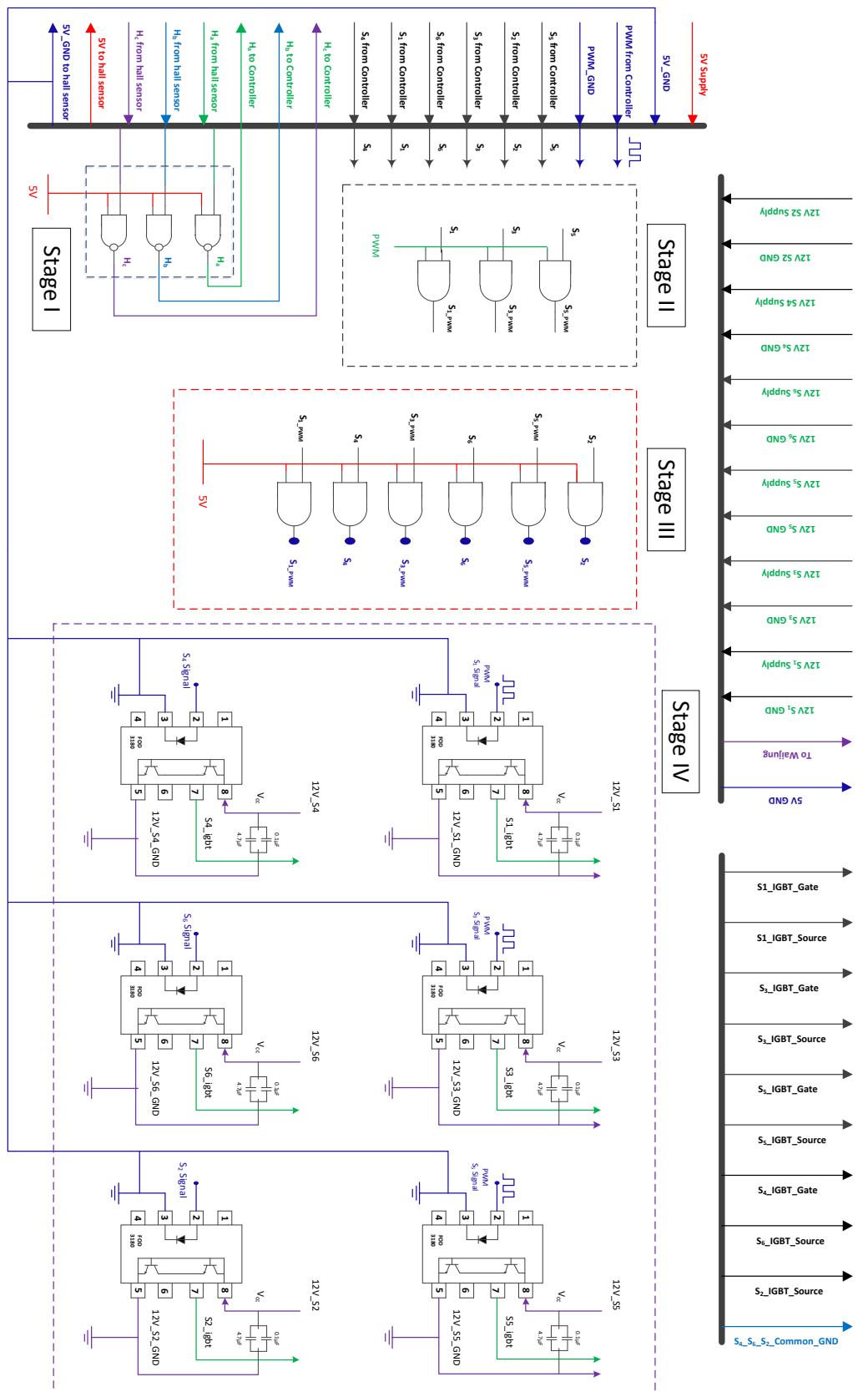


Figure 5.4: Block Diagram of Decoder Circuit

5. Hardware

5.4 Open loop hardware implementation

A block diagram representation of the open-loop implementation is shown in Fig. 5.5. The output from the Hall-effect sensors of the BLDC motor is fed to the microcontroller through digital input pins PC10, PC11, and PC12. Based on these Hall-effect sensor input signals, the gating pulses generated by the control circuit are given to the appropriate switches of the inverter, which feeds the BLDC motor. The upper switches, where the PWM signal is provided, are given through the PWM pins PC6, PC7, and PC8 of the microcontroller. For the lower switches, the digital output ports of the microcontroller (PD2, PD11, and PD13 pins) are used to feed signals to the inverter [25].

A push-pull button PD7 was used to provide control over the system. Switching pulses were generated only after pressing the PD7 control button, as all the switching signals were multiplied with the control signal and then fed to the microcontroller.

Once the electronic commutation logic was established, resulting in the generation of six switching pulses, the next step involved incorporating pulse width modulation (PWM) exclusively for the upper switches. This required providing a constant duty cycle and integrating the effect of PWM alongside the electronic commutation effect for the upper switches. To achieve this, an AND gate was employed, enabling the synchronisation of the PWM signal with the electronic commutation logic. This approach ensured precise control over the motor's speed and performance while effectively managing power consumption.

In order to display important parameters of the model, the LCD setup of the microcontroller was utilized. Within this setup, the values of the duty ratio and the ON/OFF status were displayed.

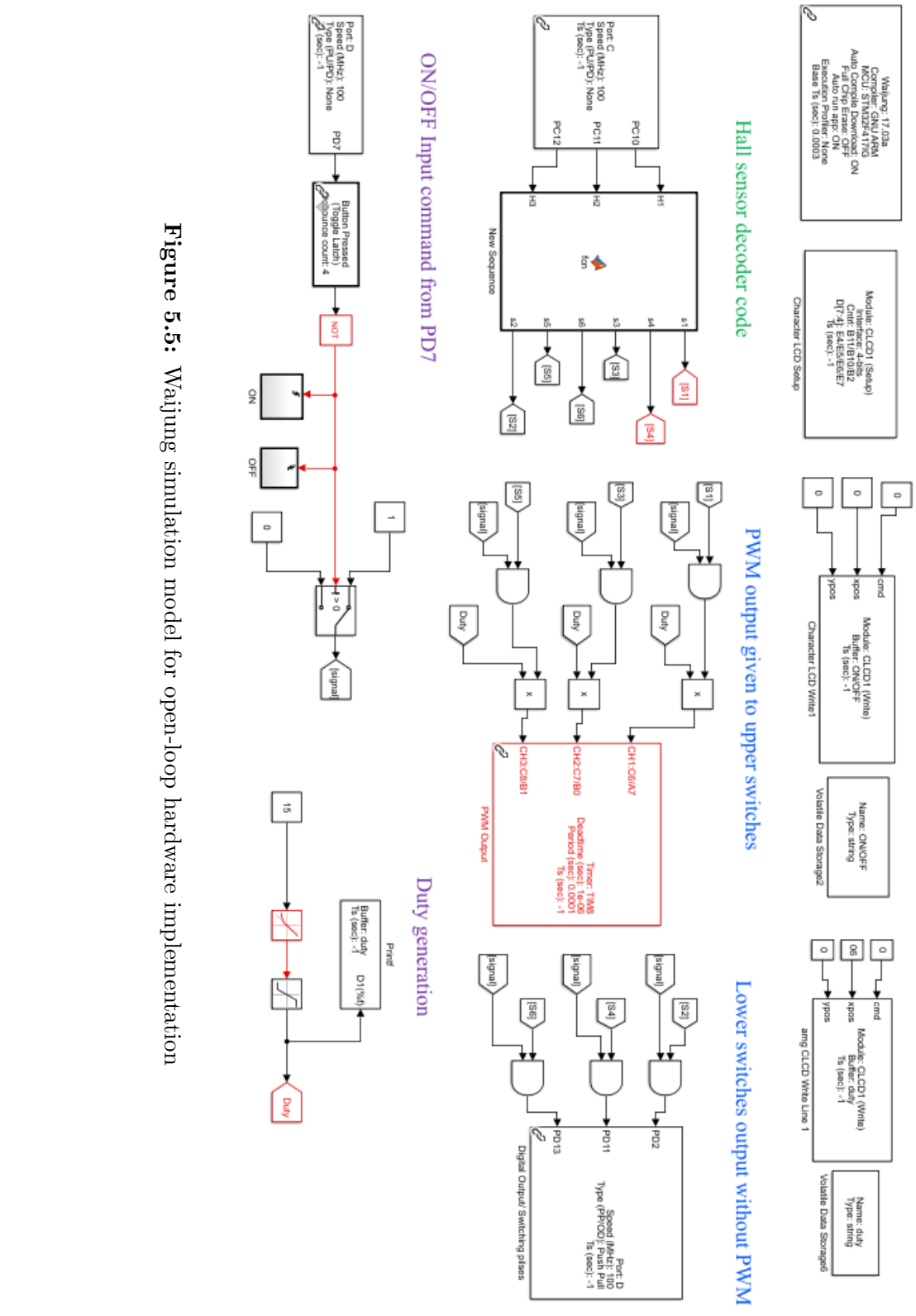


Figure 5.5: Wajung simulation model for open-loop hardware implementation

5. Hardware

5.4.1 Open loop results

While hardware implementation of BLDC motor in open loop, the waveform of the input side DC current has also been observed for various duty ratio values, ranging from 25% to 40%.

Note: Duty is applied to channel 1 of the CRO, while the input side DC current is fed into channel 3 of the CRO.

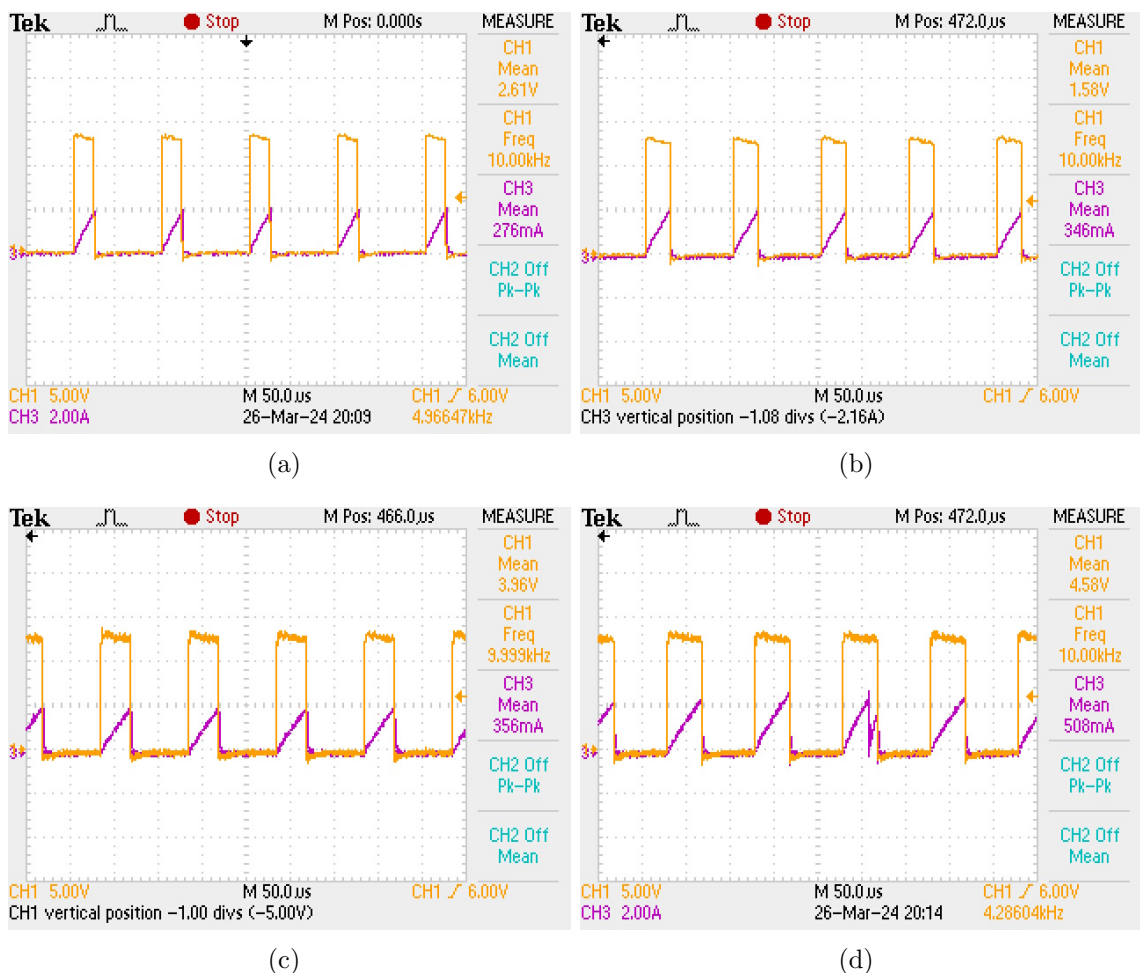


Figure 5.6: Input side DC current for different value of duty: (a) when duty is 25% (b) when duty is 30% (c) when duty is 35% (d) when duty is 40%

As per the above waveform, the battery current waveform has some positive values only for the ON duration of the applied duty cycle. This is because for the BLDC motor to operate at any particular instant, only one phase has to be energised. Therefore, if the

switch for that particular phase is off due to the PWM technique, it will act like an open circuit, and there will be no current from the battery side.

The table below represents the variation of speed with respect to duty variation in the hardware implementation of a BLDC motor operating in an open-loop system:

Duty (in %)	Speed (in rpm)
15	76
20	117
25	156
30	190
35	218
40	247
45	273
50	293

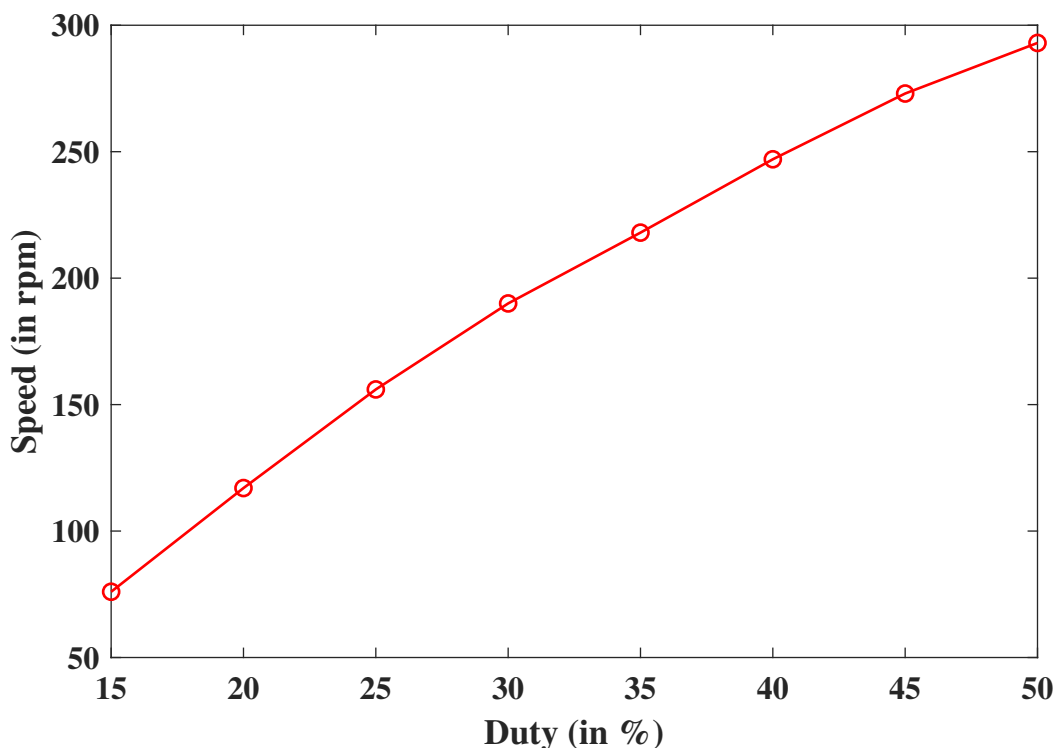


Figure 5.7: Plot representing variation of speed with respect to duty variation

5. Hardware

5.5 Close loop hardware implementation

The implementation of Brushless Direct Current (BLDC) motor control systems is a critical area in modern electrical engineering, particularly for applications requiring high efficiency, reliability, and performance. This report delves into the hardware implementation of a BLDC motor control system utilising the Waijung Blockset, a versatile and powerful tool integrated with MATLAB/Simulink. The Waijung Blockset facilitates rapid prototyping and deployment of complex control algorithms onto embedded hardware platforms, enabling efficient and streamlined development processes. By leveraging this block set, the project aims to achieve precise control over the BLDC motor, ensuring optimal performance and demonstrating the practical applications of model-based design in advanced motor control systems [25].

As we have already discussed in the open loop implementation section, we used the Waijung Blockset to generate the code that can be loaded onto the STM32 microcontroller. We also used the PWM technique in the open loop implementation, but we provided a constant duty ratio. Now, in the closed-loop implementation, the duty ratio value will be obtained from the output of the controller.

In the closed-loop implementation, the reference speed was first compared with the actual speed to generate the error signal. This error signal was then given to the PI controller, which generated the required duty ratio. The parameters of the PI controller were decided by observing the open-loop results. First, the value of K_P was determined by analysing the speed vs duty plot that was generated for different values of duty ratio during the open-loop hardware implementation. Once the value of K_P was obtained, the value of K_I was determined by considering the transient and steady-state performance of the motor.

Figure 5.8 shows the Waijung model of the closed-loop speed control of the BLDC motor, where the reference speed was successfully achieved using a linear controller, specifically a PI controller, with fine-tuning.

5.5 Close loop hardware implementation

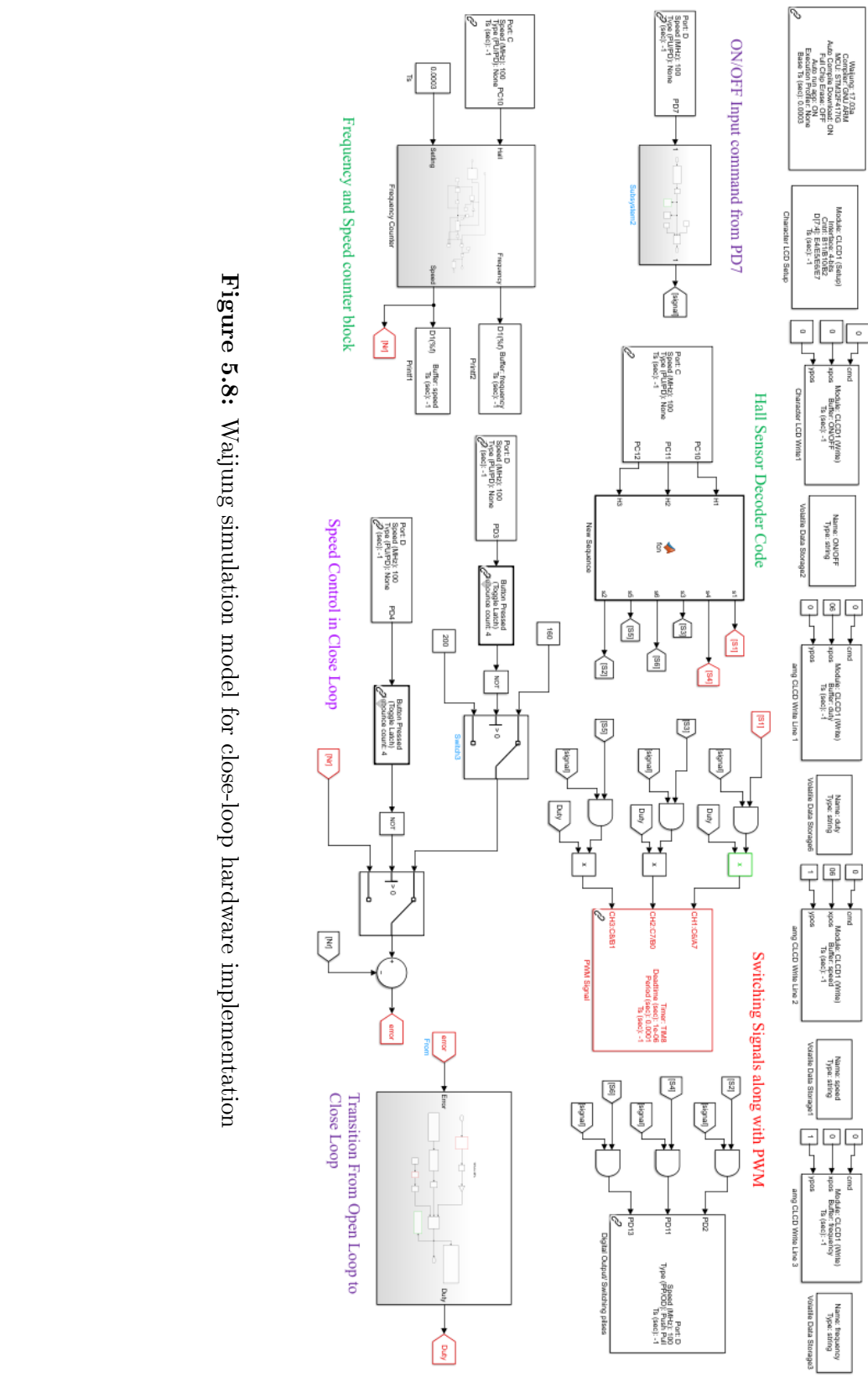


Figure 5.8: Waijung simulation model for close-loop hardware implementation

5. Hardware

To perform speed control of the BLDC motor, first, the actual speed should be known that can be compared with reference speed to generate duty. The actual speed of the motor can be easily found by the speed sensor, but we tried to perform speed control without a speed sensor to minimise the cost of the project. So, the main challenge was to find the speed from the waveform of the hall sensor.

Hall sensors generate a digital pulse which has a particular frequency, and that frequency varies based on speed variation. So the idea was if we were able to find the frequency of the hall sensor, then we could easily calculate the speed of the motor by the given formula:

$$N_r = \frac{120f}{P}$$

Where f is the calculated hall sensor frequency and P is the number of poles.

5.5.1 Frequency counter

The output of one of the Hall sensors is fed to the edge detector block, which can detect both rising and falling edges. The output of the edge detector is then sent to the up counter. If we use a rising edge detector block, the counter will start counting upon detecting a rising pulse and will continue counting until the next rising edge. When the next rising pulse is detected, the counter will reset automatically and start counting from 0 again.

In this way, we get the count value for an entire time period of the Hall sensor. An Enabled Subsystem block in Simulink is then used to calculate the time period from the count value. This calculated time is multiplied by the sampling time to get the total time period of the Hall sensor. Once we have the time period, we simply invert it to get the frequency of the Hall sensor.

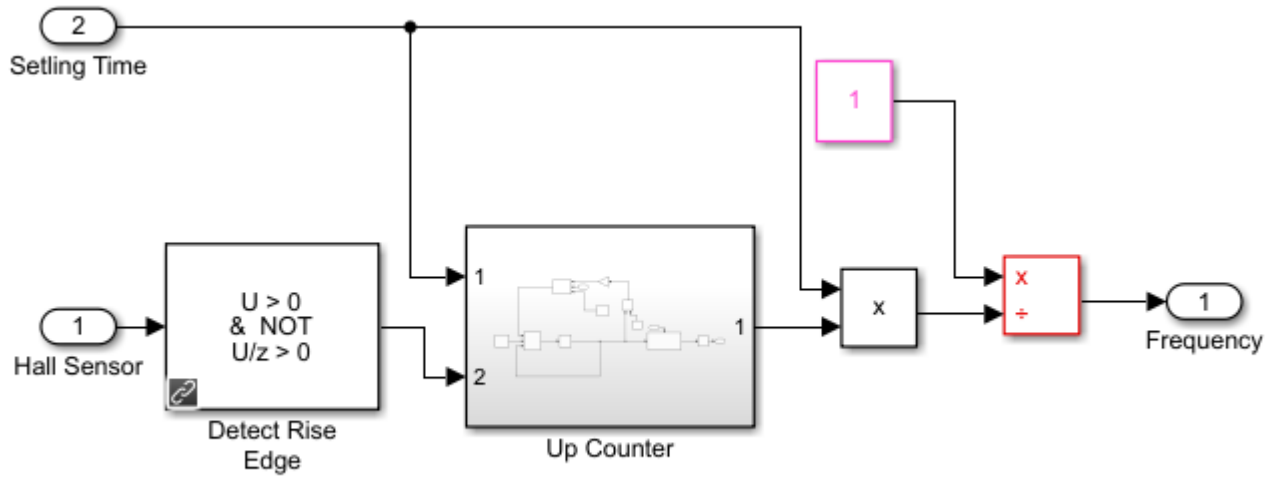


Figure 5.9: Frequency counter

5.5.2 Waijung Simulation

Closed-loop control is implemented in such a way that there will be a control button. After pressing it, the closed-loop control will start. Before that, the system will operate in open loop only with fixed duty ratio. We used the PD6 button of the Waijung Blockset for this control button.

5. Hardware

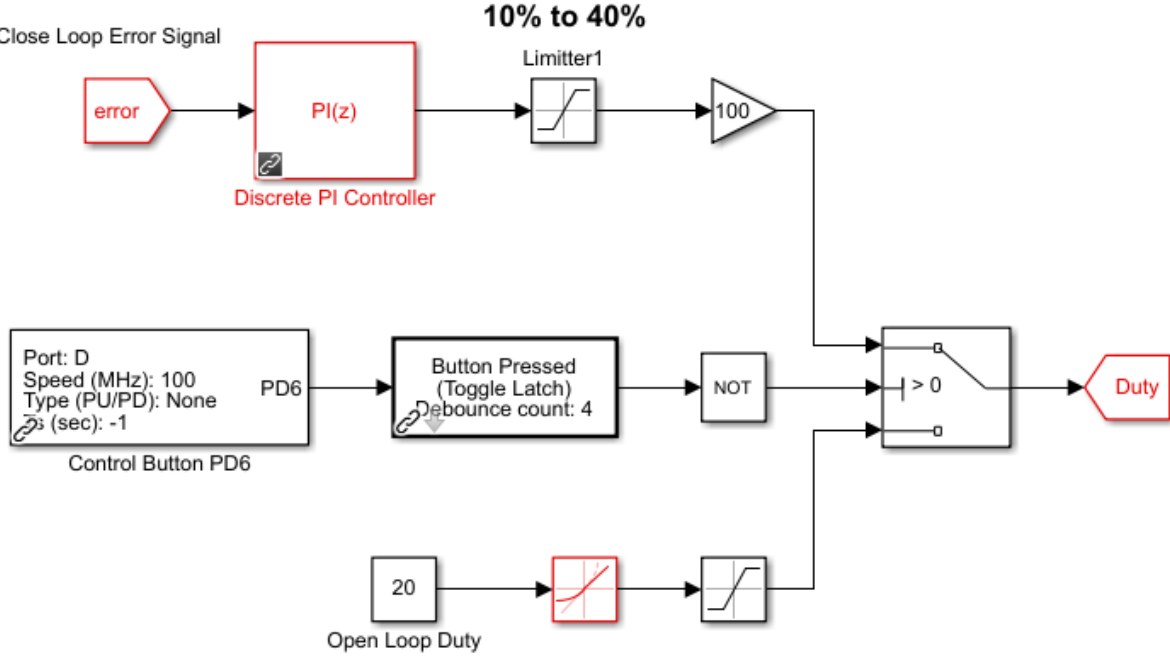


Figure 5.10: Circuit which switches operation from open to close loop

In closed-loop operation, the error signal is generated by comparing the reference speed with the calculated actual speed. This error signal is then given to the PI controller, which generates the required duty value.

5.5.3 Speed range

When the system transitions from open-loop to closed-loop control, the duty cycle suddenly increases to its maximum value, causing a large, undesirable speed variation. To overcome this problem, we use a control switch, PD4, of the Wajung Blockset.

When the system moves to closed-loop operation, it initially operates at the same speed as it was in the open loop. Only after pressing the control button PD4 will it adjust to the desired speed in closed-loop operation. In this way, we have performed the close-loop control in a more efficient way.

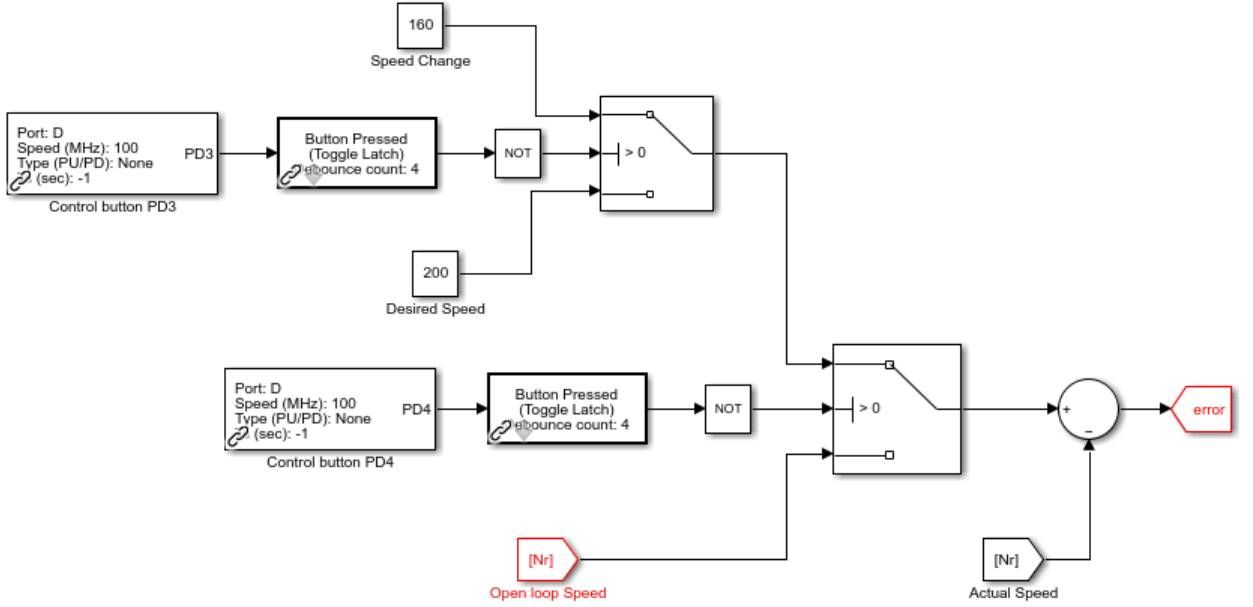


Figure 5.11: Speed range in close-loop operation

After pressing the control switch PD4, the desired speed is passed through the switch, where it is compared with the actual speed to generate an error signal.

5.5.4 Digital to Analog Converter (LTC2645)

The LTC2645 is a family of dual 12-, 10-, and 8-bit PWM to-voltage output DACs, which measures the period and pulse width of the PWM input signals and updates the voltage output DACs after each corresponding PWM input rising edge. It converts a PWM input to an accurate, stable, buffered voltage without the latency, slow settling, and high value passive components required for discrete solutions. The PWM input pins (INX) accept frequencies from 30Hz up to 6.25kHz (12-bit), 25kHz (10-bit), or 100kHz (8-bit).

The LTC2645 IC is used to plot the internally calculated speed for different duty cycles in both open and closed-loop implementations. The speed is first given to the PWM block of the Waijung Blockset, which generates a pulsating signal as the output. This pulsating signal is then provided as input to the DAC LTC2645. After making all other connections correctly, we observed the output of this converter on the CRO.

5. Hardware

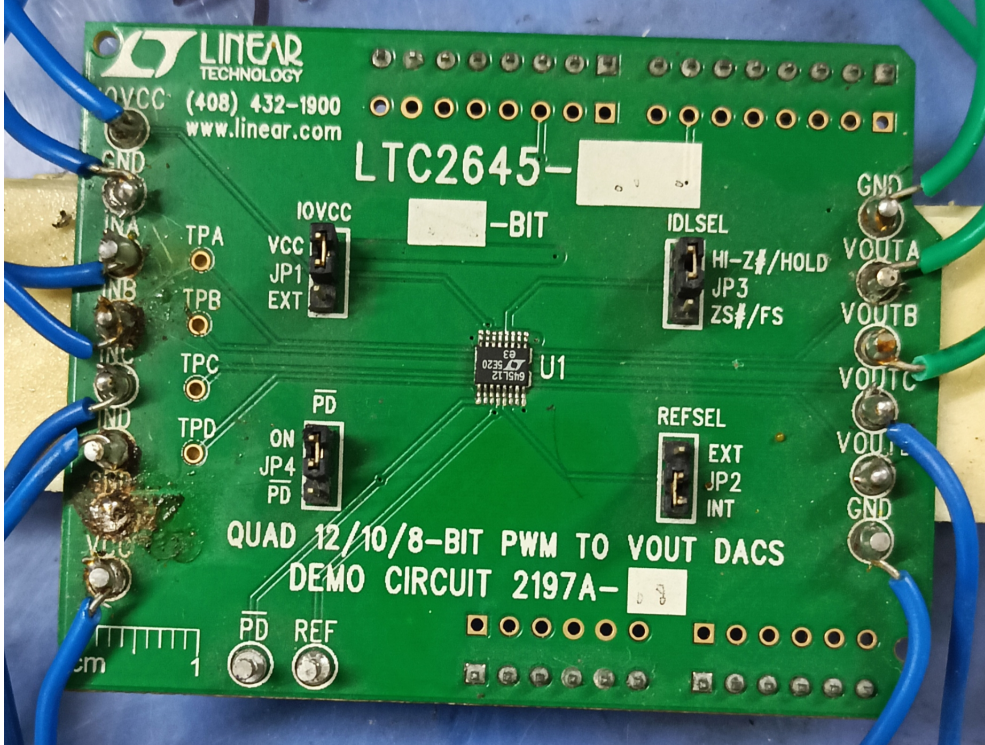


Figure 5.12: Digital to Analog converter LTC2645

The duty cycle is calculated after each PWM input rising edge based upon the previous high and low pulse width. The resulting digital DAC code k is calculated as:

$$k = 2^N * \frac{t_{PWX}}{t_{PERX}}$$

where t_{PWX} is the pulse width of the signal and t_{PERX} is the time period of the digital signal. The digital-to-analog transfer function is:

$$V = \left(\frac{k}{2^N}\right) V_{REF}$$

for $k = 0$ to $2^N - 1$

Where N is the resolution, V_{REF} is 2.5V for internal reference mode or the REF pin voltage for external reference mode.

Pin Diagram

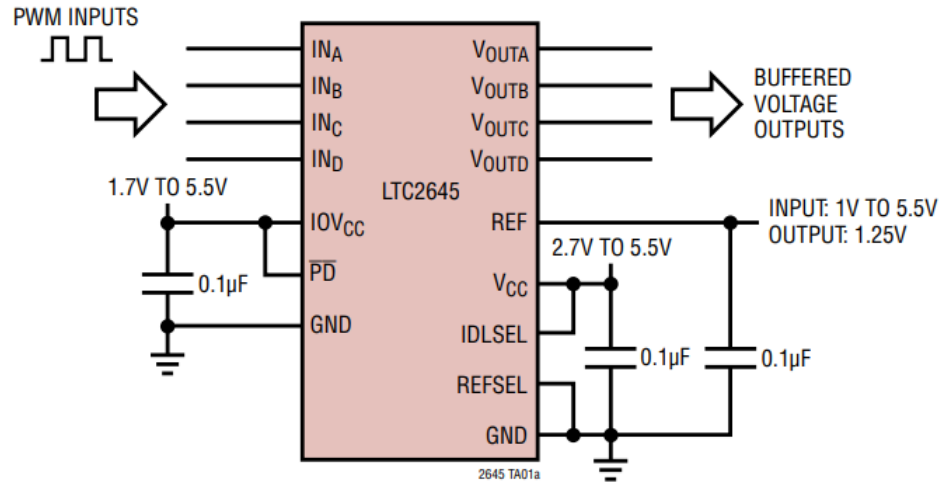


Figure 5.13: Pin diagram of DAC converter LTC2645

- IOVCC is connected to supply (1.7V to 5.5V).
- VCC port is sorted to IOVCC terminal through jumper wire.
- PD terminal is connected to ON port through jumper wire.
- REFSEL terminal is connected to INT port through jumper wire.
- IDLSEL terminal is connected to HI-Z/HOLD port through jumper wire.
- INA, INB, INC and IND are the four input channels where digital input can be provided.
- VOUTA, VOUTB, VOUTC, and VOUTD are the four corresponding output channels from which Analog output can be obtained.
- There are four GND terminals, two input and two output sides. All GND terminals are sorted to each other.

5. Hardware

5.5.5 Hardware Results

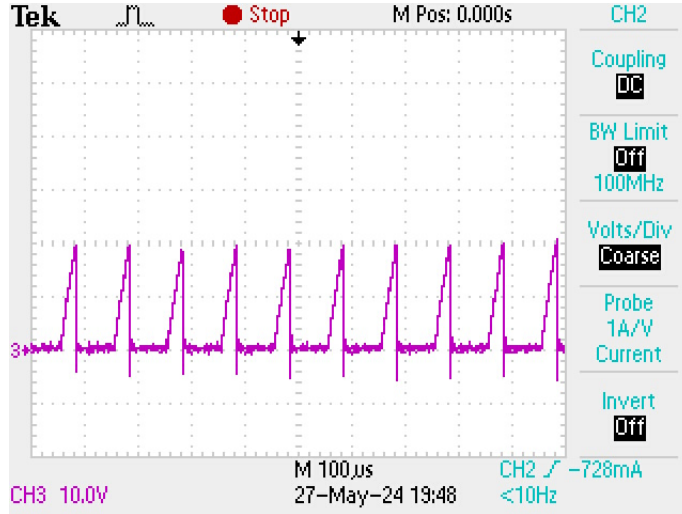


Figure 5.14: Battery current

From the battery current waveform, we can observe that it has some positive values for certain instants and zero values for other instants. The reason for this is that for the BLDC motor to operate at any particular instant, only one phase has to be energised. Therefore, if the switch for that particular phase is off due to the PWM technique, it will act like an open circuit, and there will be no current from the battery side.

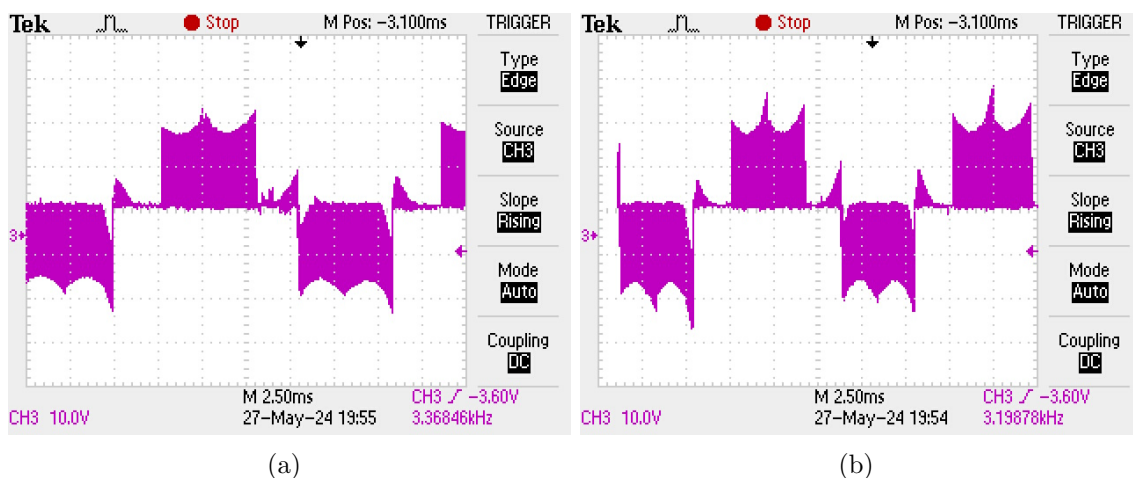


Figure 5.15: Stator current when: (a) Speed is 160 rpm (b) Speed is 200 rpm

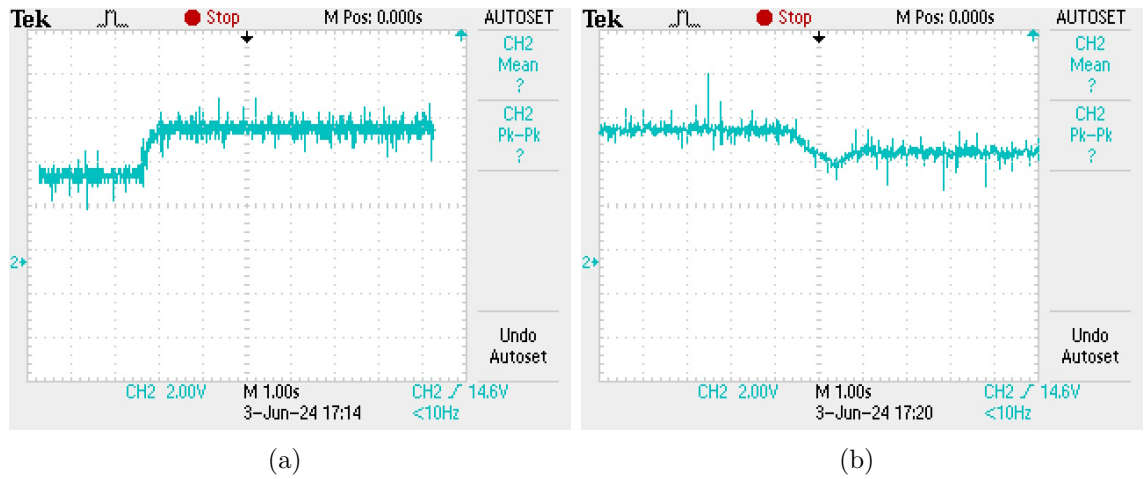


Figure 5.16: (a) Variation of speed from open loop to close loop operation (115rpm to 200rpm)(b) Speed changes in close loop (200rpm to 160rpm)

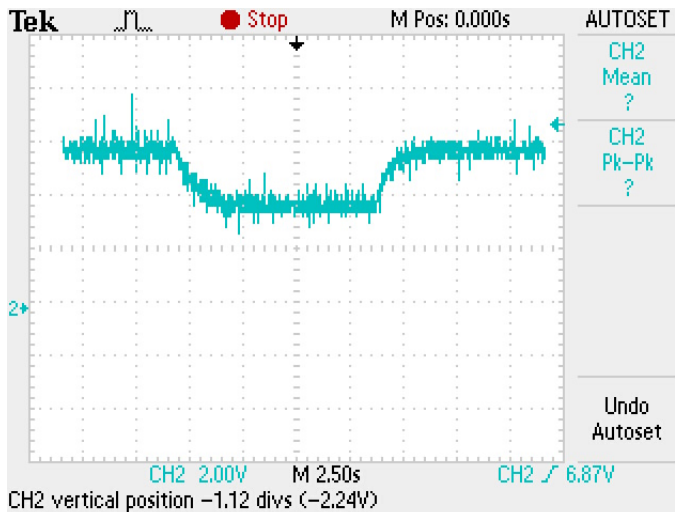


Figure 5.17: Speed variation from close loop to open loop and then again to close loop

From the stator current waveform, we can observe that when speed increases, the time period of the waveform decreases, and hence frequency increases.

In this hardware setup, the BLDC motor is operated in 120° commutation. Each switch operates for only 120° and turns off for the remaining 60° . In the shown waveform, the battery current waveform is more zoomed in than the stator current waveform because the time period of the stator current waveform is in milliseconds, while the battery current waveform is in microseconds. The battery current waveform is shown during the PWM action, resulting in positive values for the battery current only during the ON duration.

5. Hardware

6

Conclusion and Future Scope

Contents

6.1 Conclusion	82
6.2 Future Work	82

6. Conclusion and Future Scope

6.1 Conclusion

This project analyses the theory around Brushless DC (BLDC) motors, including dynamic modelling and several commutation modes. Both the 120° conduction and 180° conduction modes of BLDC motor operation have been theoretically analysed. Furthermore, effective closed-loop and open-loop simulations for both 120° commutation and 180° commutation modes have been carried out with the MATLAB/Simulink framework.

Theoretical analysis of different control techniques, including DC current control, field-oriented control(FOC) and hysteresis current control, has been successfully analysed, and the FOC technique is used to perform the close loop simulation of BLDC motor for both 120° conduction and 180° conduction mode. In order to obtain controller parameters, the Ziegler-Nichols tuning method has also been analysed.

Finally, the implementation of the speed control of the BLDC motor using the Wajung Blockset and STM32F4 Discovery board was introduced and carried out. Due to its low cost and simple design, the STM32F4-Discovery combined with the Wajung environment can be considered an ideal platform for the implementation of command and control algorithms for the BLDC motor. Simulation and experimental tests were conducted for speed variation at no load. These results showed a very significant correlation between MATLAB/Simulink Wajung Blockset and the STM32F4 controller without the need for writing computer programs. All results demonstrated the efficiency and accuracy of the proposed algorithm, especially the PI controller.

6.2 Future Work

Future Works Include The Following:

- Speed control of the BLDC motor will be performed using different controller design techniques such as sliding mode control, and the performance will be compared with that of a linear PI controller.
- Hardware implementation of field oriented control (FOC) will be performed using

STM32F407G microcontroller in a 2 kW scaled-down hardware set-up in the laboratory with a wheel-hub motor.

6. Conclusion and Future Scope

References

- [1] V. Bist and B. Singh, "Pfc cuk converter-fed bldc motor drive," *IEEE Transactions on Power Electronics*, vol. 30, no. 2, pp. 871–887, 2015.
- [2] S. Sakunthala, R. Kiranmayi, and P. N. Mandadi, "A study on industrial motor drives: Comparison and applications of pmsm and bldc motor drives," in *2017 International Conference on Energy, Communication, Data Analytics and Soft Computing (ICECDS)*, 2017, pp. 537–540.
- [3] M. Lazor and M. Stulrajter, "Modified field oriented control for smooth torque operation of a bldc motor," in *2014 ELEKTRO*, 2014, pp. 180–185.
- [4] Q. Han, N. Samoylenko, and J. Jatskevich, "Average-value modeling of brushless dc motors with 120-degree voltage source inverter," in *2008 IEEE Power and Energy Society General Meeting - Conversion and Delivery of Electrical Energy in the 21st Century*, 2008, pp. 1–1.
- [5] R. Krishnan, *Permanent magnet synchronous and brushless DC motor drives*. CRC press, 2017.
- [6] B. Hu, S. Sathiakumar, and Y. Shrivastava, "180-degree commutation system of permanent magnet brushless dc motor drive based on speed and current control," in *2009 Second International Conference on Intelligent Computation Technology and Automation*, vol. 1, 2009, pp. 723–726.
- [7] G. Krishnan and K. T. Ajmal, "A neoteric method based on pwm on pwm scheme with buck converter for torque ripple minimization in bldc drive," in *2014 Annual International Conference on Emerging Research Areas: Magnetics, Machines and Drives (AICERA/iCMM&D)*, 2014, pp. 1–6.
- [8] H. Cao, S. Huang, Z. Yan, X. Li, G. Zhang, and W. Zhang, "Research on 180° conduction of brushless dc motor driven by high frequency link inverter," in *2017 IEEE Transportation Electrification Conference and Expo, Asia-Pacific (ITEC Asia-Pacific)*, 2017, pp. 1–6.
- [9] Q. Han, N. Samoylenko, and J. Jatskevich, "Comparison of brushless dc motor drives with 180/120-degree inverter systems," in *2007 Canadian Conference on Electrical and Computer Engineering*, 2007, pp. 111–114.
- [10] G. Meng, H. Xiong, and H. Li, "Commutation torque ripple reduction in bldc motor using $pwm_{on}pwm$ mode," in *2009 International Conference on Electrical Machines and Systems*, 2009, pp. 1–6.
- [11] H. S. Chuang, Y.-L. Ke, and Y. C. Chuang, "Analysis of commutation torque ripple using different pwm modes in bldc motors," in *Conference Record 2009 IEEE Industrial & Commercial Power Systems Technical Conference*, 2009, pp. 1–6.

REFERENCES

- [12] K. Ogata, *Modern control engineering fifth edition*, 2010.
- [13] Z. Wang, S. Qiu, R. Song, X. Wang, B. Zhu, and B. Li, “Research on pid parameter tuning of coordinated control for ultra-supercritical units based on ziegler nichols method,” in *2019 IEEE 3rd Advanced Information Management, Communicates, Electronic and Automation Control Conference (IMCEC)*, 2019, pp. 1155–1158.
- [14] Z. Juric and B. Perunicic, “An extension of the ziegler-nichol’s method for parametric identification of standard plants,” in *Proceedings of the 12th IEEE Mediterranean Electrotechnical Conference (IEEE Cat. No.04CH37521)*, vol. 1, 2004, pp. 363–366 Vol.1.
- [15] P. Sarala, S. F. Kodad, and B. Sarvesh, “Analysis of closed loop current controlled bldc motor drive,” in *2016 International Conference on Electrical, Electronics, and Optimization Techniques (ICEEOT)*, 2016, pp. 1464–1468.
- [16] P. Mukherjee and M. Sengupta, “Closed loop speed control of a laboratory fabricated brushless dc motor drive prototype using position sensor,” in *2017 National Power Electronics Conference (NPEC)*, 2017, pp. 166–171.
- [17] M. M. R. A. Milani, T. Çavdar, and V. F. Aghjehkand, “Particle swarm optimization — based determination of ziegler-nichols parameters for pid controller of brushless dc motors,” in *2012 International Symposium on Innovations in Intelligent Systems and Applications*, 2012, pp. 1–5.
- [18] M. N. Gujjar and P. Kumar, “Comparative analysis of field oriented control of bldc motor using spwm and svpwm techniques,” in *2017 2nd IEEE International Conference on Recent Trends in Electronics, Information & Communication Technology (RTEICT)*, 2017, pp. 924–929.
- [19] B. P. Kumar and K. C.M.C, “Comparative study of different control algorithms on brushless dc motors,” in *2016 Biennial International Conference on Power and Energy Systems: Towards Sustainable Energy (PESTSE)*, 2016, pp. 1–5.
- [20] M. A. Islam, M. B. Hossen, M. S. Hasan, and B. C. Ghosh, “Field oriented rectangular current regulated pwm control of permanent magnet brushless dc motor,” in *2017 4th International Conference on Advances in Electrical Engineering (ICAEE)*, 2017, pp. 346–351.
- [21] B.-K. Lee and M. Ehsani, “Advanced simulation model for brushless dc motor drives,” *Electric power components and systems*, vol. 31, no. 9, pp. 841–868, 2003.
- [22] A. Hmidet and O. Hasnaoui, “Wajjung blockset-stm32f4 environment for real time induction motor speed control,” in *2018 IEEE 5th International Congress on Information Science and Technology (CiSt)*, 2018, pp. 600–605.
- [23] P. Chaturvedi, M. A. Mulla, and S. K. Patro, “Power electronics laboratory education using arm cortex m4 32-bit microcontroller,” in *2018 IEEE International Conference on Power Electronics, Drives and Energy Systems (PEDES)*, 2018, pp. 1–6.
- [24] B. Mirac and A. Kilic, “Assessment of several pid controllers applied to dc motors,” in *2021 5th International Symposium on Multidisciplinary Studies and Innovative Technologies (ISMSIT)*, 2021, pp. 700–705.
- [25] J. A. Reshi and R. K, “A novel logical band approach for bldc motor speed control,” in *2022 1st International Conference on Sustainable Technology for Power and Energy Systems (STPES)*, 2022, pp. 1–6.